Earth Departure Trajectory Reconstruction of Apollo Program Components Undergoing Disposal in Interplanetary Space

Introduction

A total of six Apollo Program components were targeted for disposal in interplanetary space during mission operations. Five of these components are Saturn V launch vehicle third stages, known as the Saturn IV-B (S-IVB), associated with missions Apollo 8, Apollo 9, Apollo 10, Apollo 11, and Apollo 12. The Apollo 10 Lunar Module ascent stage (LM) was also targeted for interplanetary space disposal following crewed operations in lunar orbit.*

As will be documented in this paper, all six disposed objects initially departed Earth's vicinity with relatively low geocentric energy, achieving heliocentric orbits very similar to Earth's. Myriad near-Earth objects (NEOs) also occupy such orbits. Many NEOs tens or a few hundreds of meters in size have yet to be detected, or their locations are highly uncertain even a few years before or after discovery [1, Chapter 3]. Those NEOs in Earth-similar orbits are also the most accessible interplanetary destinations for human space flight [2, 3].

The primary objective of this study is to reconstruct an Earth departure trajectory for each of the six Apollo Program components now thought to be in heliocentric orbit. Ideally, this will permit any sufficiently correlated NEO orbit to be reclassified as that of an artifact.

As-flown Apollo Program trajectory data are available to present-day researchers only as esoteric elements in the NASA Apollo trajectory (NAT) format. A process whereby NAT elements can be used to reconstruct reasonably accurate trajectories has been documented [4] and is applied throughout this study to produce initial conditions for trajectory prediction at epoch t_0. These initial conditions are specified as Cartesian position $\boldsymbol{r} \equiv [r_1, r_2, r_3]^T$ and velocity $\boldsymbol{v} \equiv [v_1, v_2, v_3]^T$ whose components are expressed in the Earth mean equator and equinox of epoch J2000.0 coordinate system (J2K). Nomenclature associated with NAT elements is as follows.

- $h \equiv$ geodetic or selenocentric altitude† in nm‡
- $\phi \equiv$ geodetic or selenocentric latitude in deg, measured positively toward the north pole of planetary rotation
- $\lambda \equiv$ geodetic or selenocentric longitude in deg measured positively in the inertial direction of planetary rotation
- $s \equiv$ geocentric or selenocentric inertial speed in ft/s

---

* Other Apollo Program hardware certainly accompanied some of the components cited here into interplanetary space. Unfortunately, there are no empirical data relating to these objects' trajectories. Likely the largest such undocumented disposed components are four spacecraft/LM adapter (SLA) panels explosively jettisoned from each S-IVB at Command-Service Module (CSM) separation during trans-lunar coast. Although these jettisons were performed on missions Apollo 8 and Apollo 10 through Apollo 17, missions Apollo 13 through Apollo 17 targeted S-IVB disposal via lunar impact. In any of these cases, zero to four SLAs may have entered interplanetary space.

† Geodetic altitude is referred to the Fischer Ellipsoid of 1960 [5, p. 2-1]. This geoid has equatorial radius = 6378.166 km and flattening factor = 1/298.3 [6]. Selenocentric altitude is referred to a sphere [7, p. 5-1]. A lunar radius of 1738.088 km is inferred from equivalent selenocentric Cartesian position components and height data generated by the Real Time Computer Complex (RTCC) during Apollo 8 [8, p. A-10].

‡ The "nm" abbreviation for "nautical miles" is used throughout this paper in accord with Apollo Program documentation.

$\gamma \equiv$ flight-path angle in deg measured positively above the local geocentric or selenocentric horizontal plane to inertial geocentric or selenocentric velocity

$\psi \equiv$ inertial heading in deg measured in the local geocentric or selenocentric horizontal plane from the projection of Earth's true north celestial pole to the projection of inertial geocentric or selenocentric velocity

The WeaveEncke algorithm [9] generates an Earth departure trajectory reconstruction (EDTR) beginning at epoch t_0 using a fixed integration step size of 120 s. Accelerations integrated during EDTR generation are limited to those of gravity from the Earth, Sun, and Moon modeled as zero-dimensional point sources. Reduced masses used for Earth, Sun, and Moon gravitation are (respectively) μ_E = 398,600.440 km^3/s^2, μ_S = 132,712,440,018. km^3/s^2, and μ_M = 4902.798 km^3/s^2 in accord with the *Horizons* on-line ephemeris system [10]. Heliocentric positions for Earth are interpolated from JPL's DE405 ephemeris downloaded at daily intervals via *Horizons*. Similarly, lunar geocentric positions are interpolated from JPL's DE405 ephemeris downloaded at hourly intervals via *Horizons*.

In general, the latest possible t_0 is selected for each EDTR based on the last available NAT elements. In many cases, an EDTR includes events at epochs t_1, t_2, … following t_0 to approximate propellant dumps and other trajectory constraints as documented by Apollo Program post-flight reports. Some impulse events are inferred by solving a perturbed Lambert problem when these reports document an accurate position, such as at pericynthion, to serve as a boundary condition at an epoch following t_0.

In addition to NAT elements, data traceable to Apollo Program post-flight documentation are frequently cited in this paper as EDTR integrity checks. Previously published post-flight data will be described as "reported" in this paper in order to distinguish them from this study's reconstructions. Unless noted otherwise, reported data comparisons with corresponding parameters derived from an EDTR should be regarded as necessary, but not sufficient, conditions indicating a degree of agreement or deviation between two trajectory reconstructions.

Two time scales published in Apollo Program reports are referenced throughout this paper. The first, Greenwich Mean Time (GMT), was equivalent to Universal Time (UT) prior to 1972. But GMT predates *Coordinated* Universal Time (UTC), which became the official civil timekeeping standard on 1 January 1972 after the disposals documented by this study were accomplished in 1968 and 1969. The second time scale is Ground Elapsed Time (GET), which measures the interval from a mission-specific launch time (*range zero* in Apollo Program documentation) to an event during that mission.

The WeavEncke algorithm uses Terrestrial Dynamical Time (TDT) as its internal time scale and is subject to the relationship TDT = UT + ΔT. As implemented for this study, ΔT is obtained from a table lookup such that ΔT = +38.29 s in year 1968 and ΔT = +39.20 s in year 1969 [11, p. K9]. These values deviate up to 0.98 s from equivalent modern data implemented in *Horizons* for 1968 and 1969. Such deviations lead to small EDTR errors from errant gravitational accelerations integrated by WeaveEncke because coordinate time (CT)[§], the DE405 ephemeris argument of interpolation, is also related to GMT through ΔT. Interpolation is most critical to EDTR fidelity during close lunar encounters, but these cases are effectively corrected by embedding perturbed Lambert solutions with reported boundary conditions at pericynthion.

With the exception of the Apollo 12 S-IVB, which did not immediately enter interplanetary space, each EDTR is terminated at the start of the next GMT day after geocentric distance first exceeds one million km. At this "Earth departure" epoch t_D, expressed with the GMT time scale, EDTR geocentric position $\boldsymbol{r}' \equiv [r_1', r_2', r_3']^T$ and velocity $\boldsymbol{v}' \equiv [v_1', v_2', v_3']^T$ are supplied by this paper as J2K Cartesian components. Providing "nominal" (best guess) t_D data in this manner leaves other researchers free to transform $\boldsymbol{r}'$ and $\boldsymbol{v}'$ to heliocentric vectors or elements using whatever value of ΔT and whatever Earth heliocentric ephemeris are deemed appropriate.

No explicit trajectory uncertainty data, such as covariance matrices, are known to be associated with the six Apollo Program components under study. In most cases, however, uncertainty magnitudes ε_r in each Cartesian component of $\boldsymbol{r}$ and ε_v in each Cartesian component of $\boldsymbol{v}$ are documented for the time frame containing t_0. Under these circumstances, a 6x6 matrix of dual-valued sensitivity coefficients m_{ij} can be generated using 12 EDTRs whose initial conditions each contain a systematic variation with respect to the nominal $\boldsymbol{r}$ or $\boldsymbol{v}$. Each variation entails subtracting (or adding) ε_r or ε_v from (or to) a nominal component of $\boldsymbol{r}$ or $\boldsymbol{v}$, respectively.

The effects of each variation are expressed as changes in the following osculating heliocentric elements at t_D with respect to their nominal values. Elements are generated using μ_S such that they reference the ecliptic and Earth mean equinox of epoch J2000.0 coordinate system (J2KE).

$EC \equiv$ eccentricity
$QR \equiv$ perihelion distance in AU
$TP \equiv$ Julian date of perihelion passage in CT
$OM \equiv$ longitude of ascending node in deg
$W \equiv$ argument of perihelion in deg
$IN \equiv$ inclination in deg

Each change in J2KE elements, normalized by $\mp\varepsilon_r$ or $\mp\varepsilon_v$ as applicable, is computed for all 12 EDTRs to produce the 6x6 matrix. Any sensitivity coefficient thereby quantifies the change in a J2KE element at t_D per unit change in an $\boldsymbol{r}$ or $\boldsymbol{v}$ J2K component at t_0. Because all J2KE elements are computed consistently among the nominal and 12 additional EDTRs, errors in ΔT and Earth's heliocentric ephemeris are considered irrelevant to m_{ij} values in this paper whose mantissas are limited to 4 digits.

As an example of sensitivity coefficient generation, consider the first two EDTRs whose variations describe the leftmost column of dual-valued sensitivity coefficients m_{i1}. These coefficients are computed using the following procedure. Any J2KE element without a sign

[§] A uniform time scale void of leap seconds, CT is used as the fundamental ephemeris argument by *Horizons*. To a precision of ±0.002 s, CT is related to international atomic time (TAI) by CT = TAI + 32.184 s.

superscript in Step 5 is associated with the nominal EDTR whose initial conditions are not subject to variations.

1) Introduce a variation to the first EDTR's initial position, computing $\boldsymbol{r}^- = [r_1 - \varepsilon_r, r_2, r_3]^T$ while leaving $\boldsymbol{v}$ with its nominal components.

2) Using the first EDTR's $\boldsymbol{r}'$ and $\boldsymbol{v}'$ at t_D, generate J2KE elements EC^-, QR^-, TP^-, OM^-, W^-, and IN^-.

3) Introduce a variation to the second EDTR's initial position, computing $\boldsymbol{r}^+ = [r_1 + \varepsilon_r, r_2, r_3]^T$ while leaving $\boldsymbol{v}$ with its nominal components.

4) Using the second EDTR's $\boldsymbol{r}'$ and $\boldsymbol{v}'$ at t_D, generate J2KE elements EC^+, QR^+, TP^+, OM^+, W^+, and IN^+.

5) Compute the leftmost column of dual-valued sensitivity coefficients as follows.

$$m_{11} = \left(\frac{EC - EC^-}{-\varepsilon_r}, \frac{EC - EC^+}{\varepsilon_r} \right)$$

$$m_{21} = \left(\frac{QR - QR^-}{-\varepsilon_r}, \frac{QR - QR^+}{\varepsilon_r} \right)$$

$$\vdots$$

$$m_{61} = \left(\frac{IN - IN^-}{-\varepsilon_r}, \frac{IN - IN^+}{\varepsilon_r} \right)$$

The second m_{i2} column of sensitivity coefficients is formed from two EDTRs with initial conditions variations confined to $r_2 \mp \varepsilon_r$ and so on until the sixth m_{i6} column is formed from two EDTRs with initial conditions variations confined to $v_3 \mp \varepsilon_v$.

In subsequent sections of this paper, the following nomenclature is used.

$C_3 \equiv$ geocentric characteristic energy, equivalent to the square of hyperbolic excess (or asymptotic) speed
$H_A \equiv$ apoapsis height
$H_P \equiv$ periapsis height

Apollo 8 S-IVB-503 Reconstruction

The Saturn V's third launch on Apollo 8 was the first to impart payload energy sufficient to reach lunar distances. Apollo 8's crewed CSM approached the Moon over its leading** hemisphere and entered lunar orbit. Using residual propellant dumps following trans-lunar injection (TLI) and

** The "leading" and "trailing" lunar hemispheres cited in this paper are with respect to the Moon's geocentric motion. They roughly correspond to western and eastern selenocentric λ, respectively.

CSM separation, the S-IVB approached the Moon over its trailing hemisphere and obtained a gravity assist leading to disposal in interplanetary space. Table 1 data recount pertinent mission events through disposal.

Table 1. The following Apollo 8 mission events led to S-IVB disposal.

GET (hhh:mm:ss)	1968 GMT	Event
000:00:00	21 Dec 12:51:00	Launch [12, p. 199]
000:11:35	21 Dec 13:02:35	Earth orbit insertion following S-IVB Burn #1: H_A = +185.18 km, H_P = +184.40 km [12, p. 201]
002:56:06	21 Dec 15:47:06	TLI following S-IVB Burn #2 [12, p. 203]
003:20:59	21 Dec 16:11:59	CSM separation from S-IVB [12, p. 203] and epoch t_0 at final published S-IVB NAT elements [5, p. 4-10]
004:55:56	21 Dec 17:46:56	S-IVB post-TLI propulsive accelerations are initiated [12, p. 201]
005:25:00	21 Dec 18:16:00	Approximate midpoint during period of post-TLI S-IVB propulsive accelerations and epoch t_1
005:38:34	21 Dec 18:29:34	S-IVB post-TLI propulsive accelerations are terminated [12, p. 201]
069:58:55	24 Dec 10:49:55	S-IVB pericynthion passage and epoch t_2: H_P = +1261 km [12, p. 202]

Table 2. Nominal geocentric initial conditions for Apollo 8 S-IVB EDTR are expressed as reported NAT elements [5, p. 4-10] and as equivalent J2K Cartesian components.

Epoch t_0 = 21 Dec 1968 at 356/16:11:59.3 GMT	
NAT Elements	**J2K Components**
h = +3797.78 nm	r_1 = -553.835328 km
ϕ = +25.863°	r_2 = -12059.904711 km
λ = -66.232°	r_3 = +5832.302535 km
s = 24,974.90 ft/s	v_1 =+4.880159164 km/s
γ = +45.110°	v_2 = -5.766576079 km/s
ψ = 107.122°	v_3 = +0.937289752 km/s

The Table 2 nominal $\boldsymbol{r}$ and $\boldsymbol{v}$ are coasted from t_0 to t_1, where geocentric position and t_1 serve as "initial" boundary conditions in a perturbed Lambert problem whose "final" boundary conditions are t_2 and selenocentric position in Table 3. A solution to this problem is sought such that deviation from Table 3 final position is less than 0.001 km.

Table 3. Selenocentric pericynthion position for the Apollo 8 S-IVB EDTR is expressed as reported NAT elements [5, p. 6-1] and as equivalent J2K Cartesian components.

Epoch t_2 = 24 Dec 1968 at 359/10:49:55.2 GMT	
NAT Elements	**J2K Components**
h = +681. nm	r_1 = -1522.470544 km
ϕ = +19.2°	r_2 = -2584.082799 km
λ = +88.0°	r_3 = +20.000528 km

The geocentric initial velocity solution to the t_1/t_2 arc's perturbed Lambert problem is equivalent to the terminal velocity of an impulse approximating all post-TLI propulsive accelerations referenced by Table 1 in the t_1 time frame. When geocentric velocity at epoch t_1, as coasted from epoch t_0, is subtracted from the Lambert solution's initial velocity at t_1, the approximating impulse's velocity increment $\boldsymbol{\Delta v}$ results. Expressed in J2K Cartesian components, nominal $\boldsymbol{\Delta v}$ = $[-0.02541585, -0.03083861, +0.02188739]^T$ km/s at t_1. This impulse is incorporated as an event in the Apollo 8 S-IVB nominal EDTR.

The magnitude $|\boldsymbol{\Delta v}|$ = 0.04556362 km/s is only slightly larger than the "longitudinal velocity increase" of 0.0419 km/s [5, p. 6-6] reported in association with all post-TLI propulsive accelerations in the t_1 time frame. Although not rigorously defined, the reported value is thought to be the body-fixed velocity change component along the S-IVB roll axis (the long cylindrical S-IVB axis of symmetry, as illustrated by Figure 1). As-flown S-IVB attitudes in the t_1 time frame with which to test this hypothesis are not known to exist. Nevertheless, the major component of $\boldsymbol{\Delta v}$ (92% of $|\boldsymbol{\Delta v}|$ in this case) is likely to lie along the S-IVB roll axis because it parallels J-2 engine thrust during Burn #1 and Burn #2.

Earth Departure Trajectory Reconstruction of Apollo Program Components Undergoing Disposal in Interplanetary Space

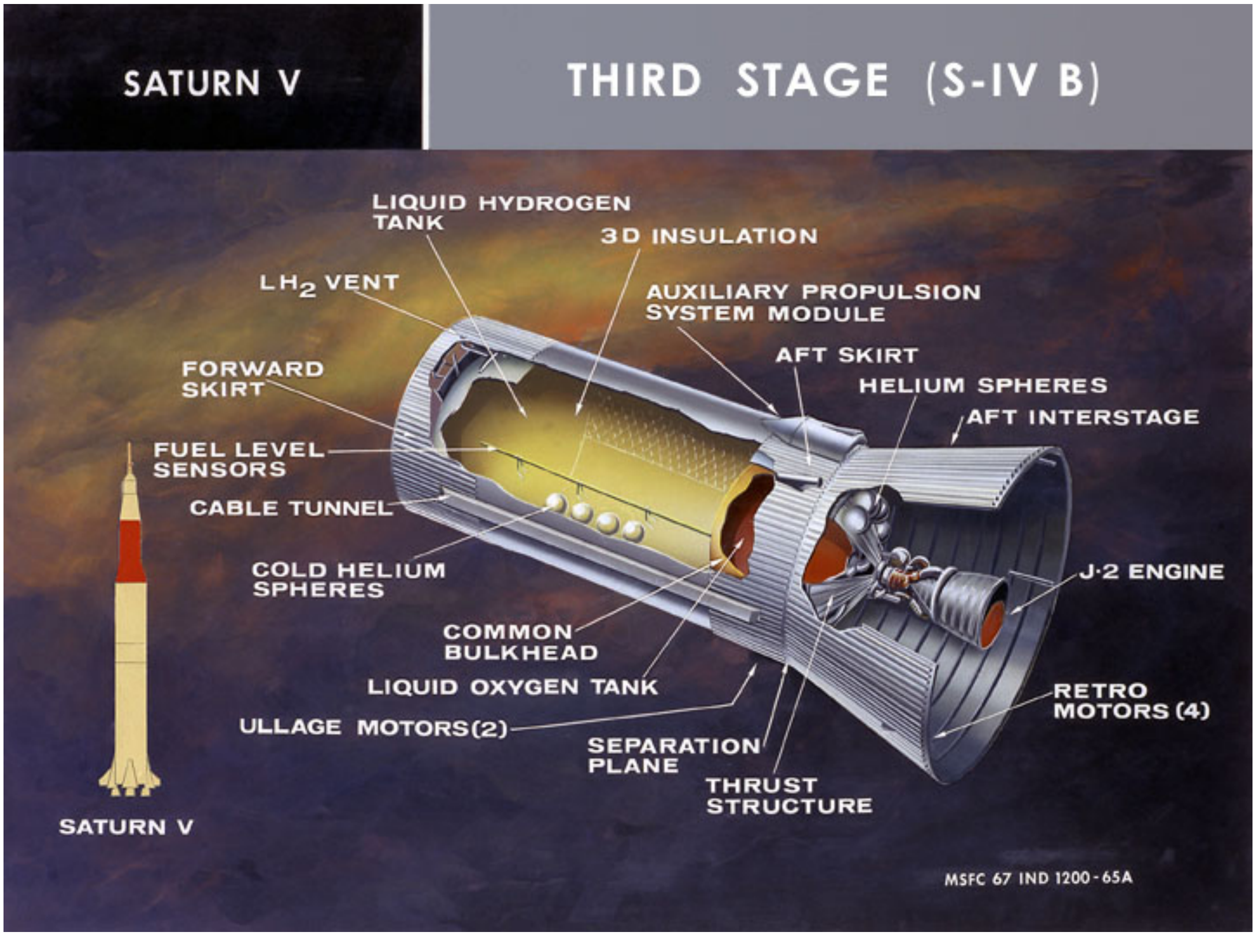

Figure 1. This Apollo Program S-IVB illustration depicts many of the propulsive components active prior to TLI and during the epoch t_1 time frame as described in Table 1 and the foregoing narrative. The "aft interstage" frustum was jettisoned at the "separation plane" using the 4 "retro motors" shortly after S-IVB Burn #1 was initiated and never reached Earth orbit.

An independent check of the t_1/t_2 arc's perturbed Lambert solution can be made because satisfied boundary values do not explicitly constrain selenocentric velocity at t_2. Since t_2 is defined to coincide with the reported pericynthion epoch, the solution's selenocentric γ at t_2 should be zero. Indeed, Lambert final selenocentric velocity (and that of the nominal EDTR) at t_2 has γ = +0.013°. Expressed in other terms, the nominal S-IVB EDTR reaches pericynthion 0.5 s before reported pericynthion at t_2.

The nominal S-IVB EDTR deviates from the reported selenocentric trajectory in one significant respect. Reported inclination referenced "to the lunar equatorial plane" is 44.56° [5, p. 6-1]. Using a more recent theory of lunar orientation [13], nominal EDTR osculating selenocentric inclination is computed to be 37.613° at t_2.

Reported S-IVB heliocentric orbit aphelion distance r_A = 147,740,000 km and perihelion distance r_P = 137,950,000 km [5, p. 6-8]. Figure 2 compares these reported apses with osculating values at hourly intervals during the nominal EDTR. As the S-IVB enters interplanetary space, Figure 2 indicates the degree to which reported apsis values are being approached asymptotically, a necessary condition for consistency.

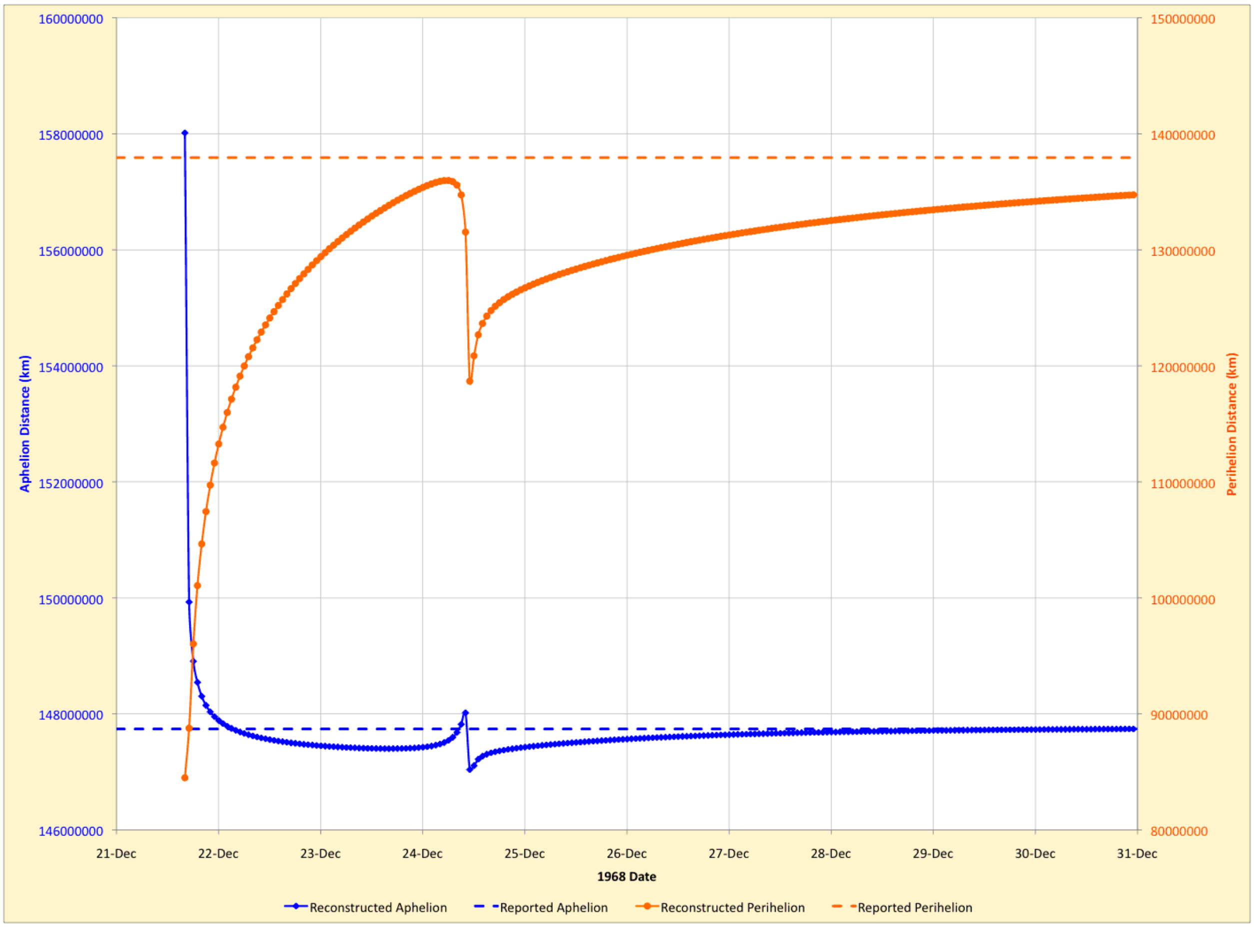

Figure 2. Apollo 8 S-IVB osculating aphelion (blue diamonds) and perihelion (orange dots) distances are plotted during nominal EDTR from 21 to 31 Dec 1968 GMT. Reported values for these apses [5, p. 6-8] are plotted as dashed lines of the corresponding color. As expected, each nominal apsis asymptotically approaches its reported value while the EDTR progresses toward interplanetary space. Rapidly varying EDTR apses on 24 Dec reflect the effects of lunar encounter.

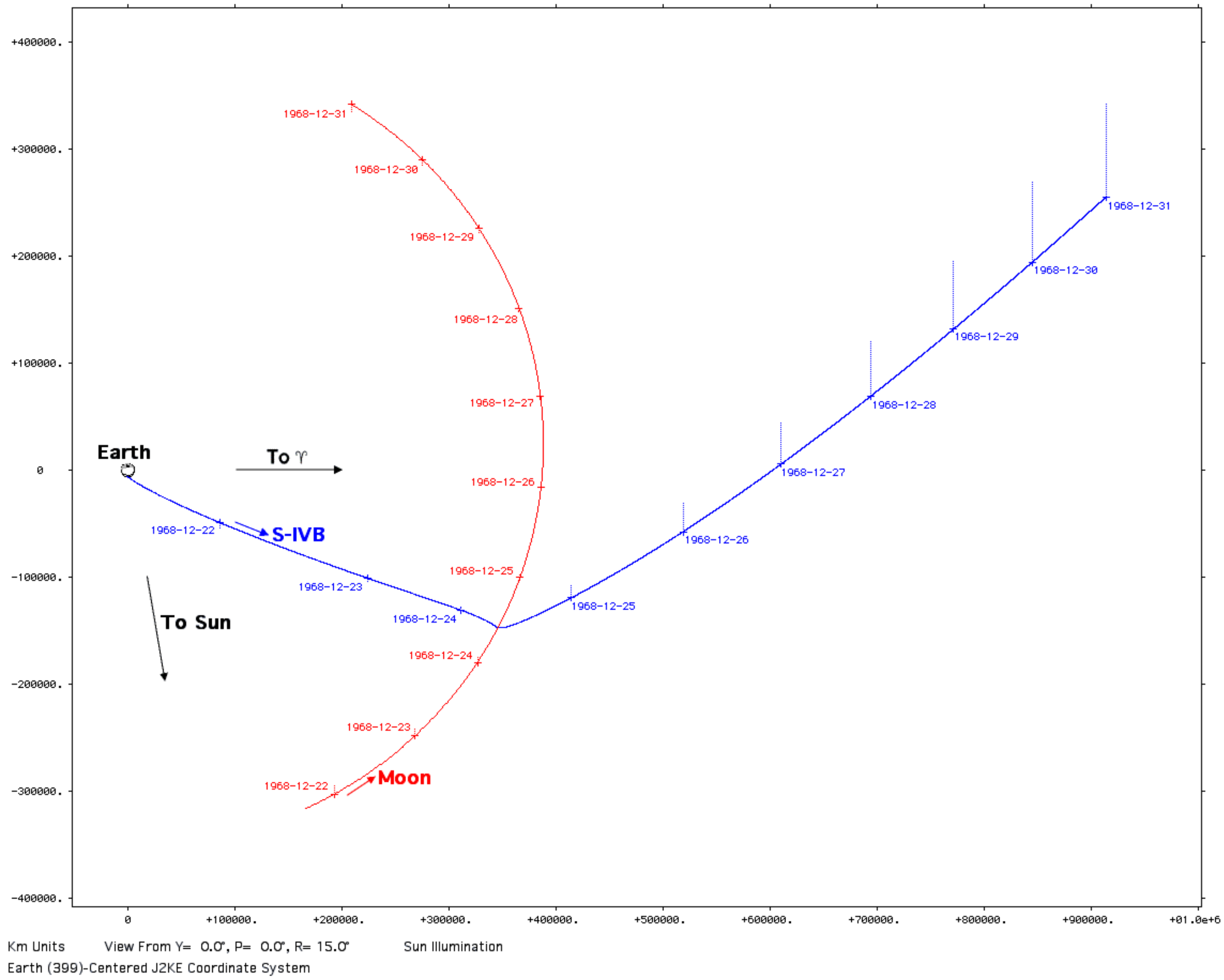

Figure 3. This geocentric inertial trajectory plot is viewed from ecliptic longitude 270°; latitude +75° and illustrates Apollo 8 S-IVB nominal EDTR. The departure asymptote lies nearly opposite Earth's heliocentric motion as inferred from the Sun's direction. Time ticks are at even GMT dates and annotated in year-month-day format. Dotted lines are projections onto the ecliptic plane.

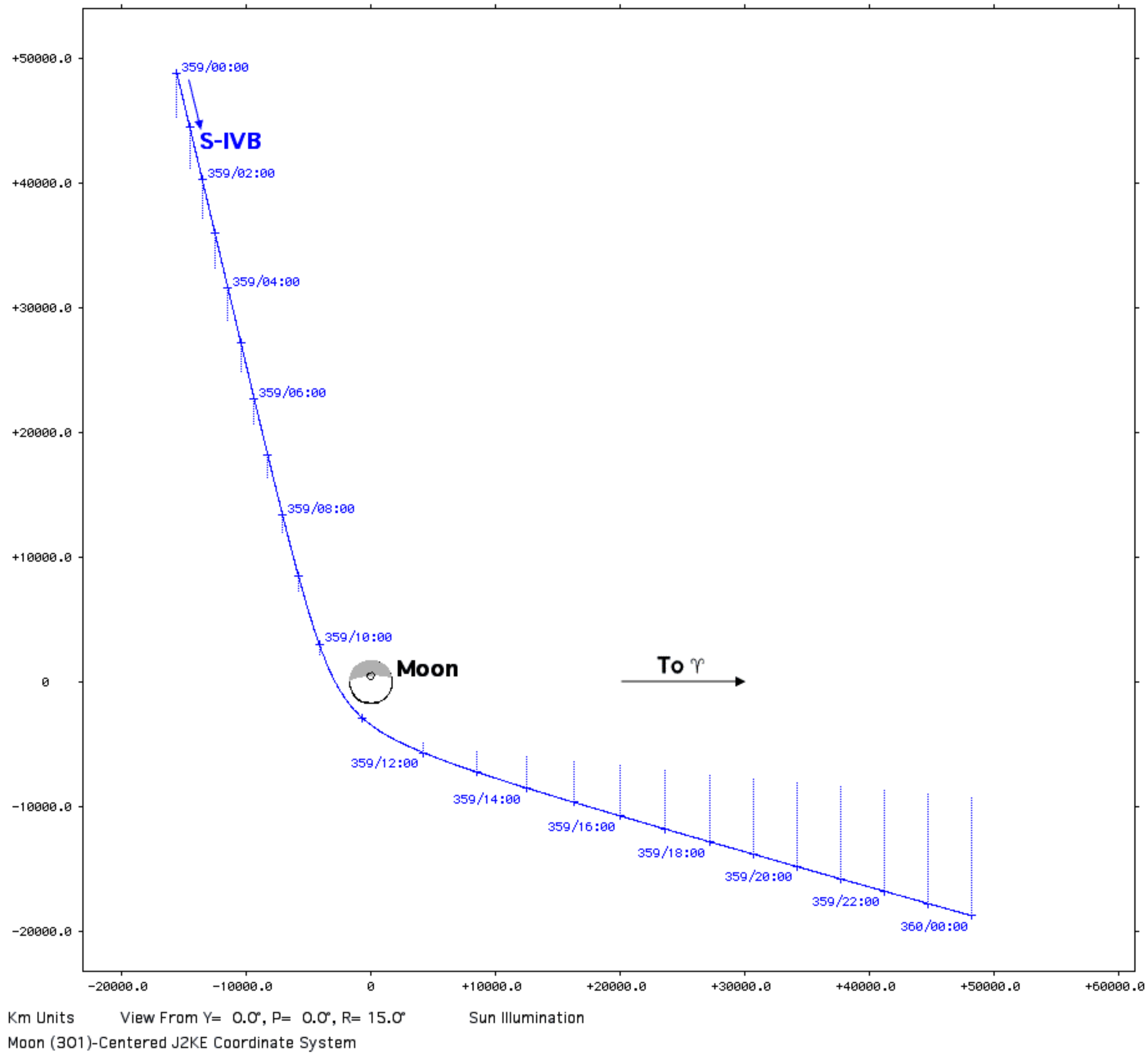

Figure 4. This inertial trajectory plot illustrates nominal Apollo 8 S-IVB EDTR selenocentric motion during 24 Dec 1968 GMT and is viewed from the same perspective as Figure 3 (ecliptic longitude 270°; latitude +75°). The Moon's shaded hemisphere is its nightside. Time tick annotations are at two-hour intervals in day-of-year/hh:mm format. Dotted lines are projections onto the ecliptic plane.

Table 4. Terminal geocentric position *r'* and velocity *v'* for the nominal Apollo 8 S-IVB EDTR are given with J2K Cartesian components.

Epoch t_D = 31.0 Dec 1968 GMT
r_1' = +914,031.468370 km
r_2' = +456,690.520138 km
r_3' = -164,522.686691 km
v_1' = +0.785912424 km/s
v_2' = +0.989024485 km/s
v_3' = -0.110977934 km/s

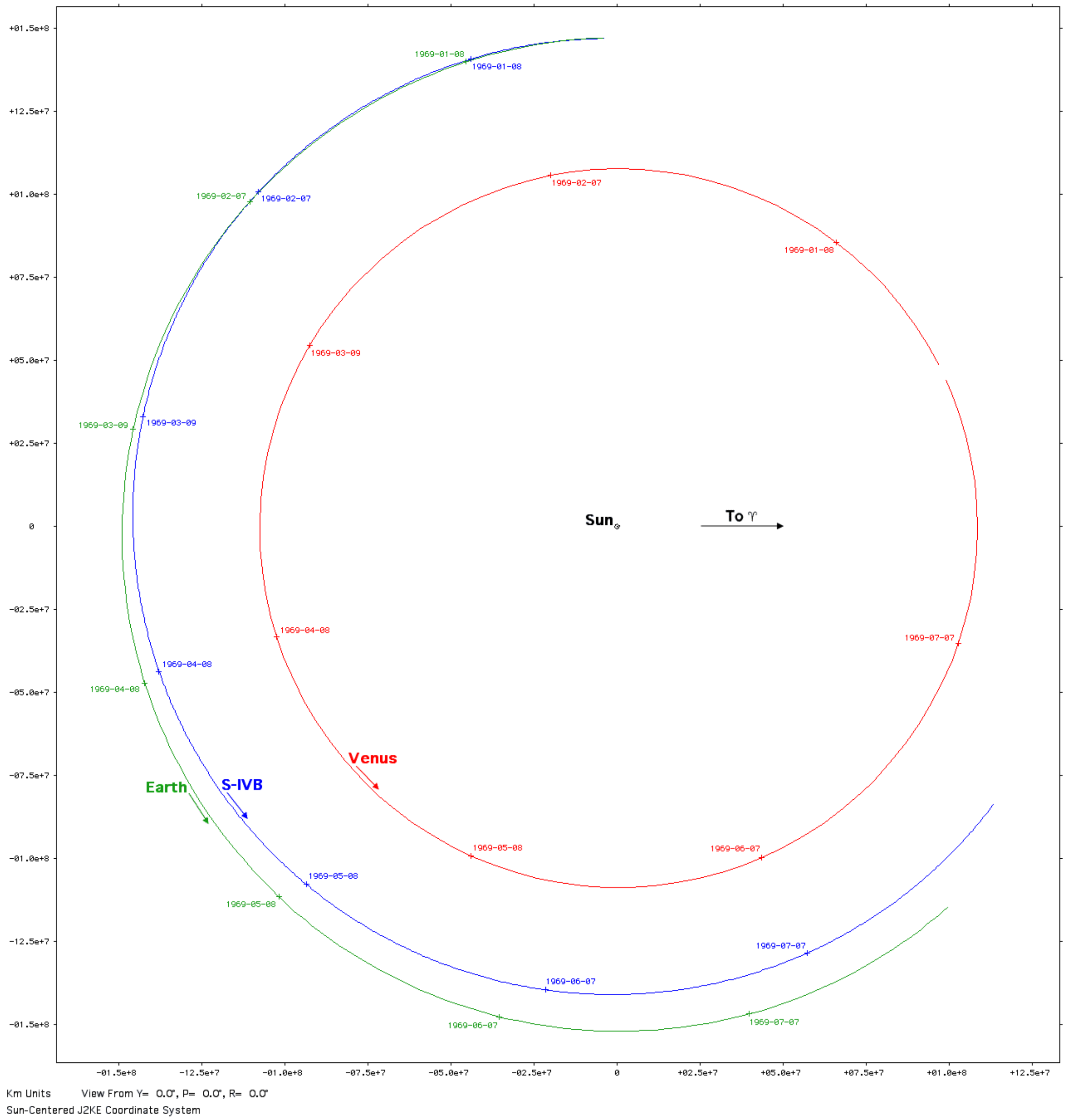

Figure 5. *Horizons* prediction of Apollo 8 S-IVB inertial heliocentric motion from Table 4 data is plotted with corresponding Earth and Venus motion for the first seven months following S-IVB disposal. Time ticks are at 30-day intervals and annotated in year-month-day format.

Total uncertainty associated with Table 2 Apollo 8 S-IVB $\boldsymbol{r}$ and $\boldsymbol{v}$ at t_0 is estimated to be $\varepsilon_r = \pm 1$ km in each position component and $\varepsilon_v = \pm 0.003$ km/s in each velocity component [5, p. 3-8]. Dual-valued sensitivity coefficients arising from ε_r variations at t_0 (m_{ij} with $i = 1 \rightarrow 6; j = 1 \rightarrow 3$) appear in Table 5, and dual-valued sensitivity coefficients arising from ε_v variations at t_0 (m_{ij} with $i = 1 \rightarrow 6; j = 4 \rightarrow 6$) appear in Table 6.

Table 5. Dual-valued sensitivity coefficients arising from ε_r variations at t_0 are presented with respect to nominal heliocentric J2KE elements at t_D.

t_0 Variations →	$r_1 \mp \varepsilon_r$	$r_2 \mp \varepsilon_r$	$r_3 \mp \varepsilon_r$
km^{-1} *EC* sensitivities	(-5.296E-08, -5.186E-08)	(2.907E-07, 2.868E-07)	(-1.158E-07, -1.149E-07)
AU/km *QR* sensitivities	(1.611E-07, 1.593E-07)	(-8.707E-07, -8.635E-07)	(3.556E-07, 3.540E-07)
day/km *TP* sensitivities	(1.773E-04, 1.778E-04)	(-9.377E-04, -9.371E-04)	(3.966E-04, 3.970E-04)
°/km *OM* sensitivities	(-1.659E-06, -1.654E-06)	(8.155E-06, 8.141E-06)	(-3.739E-06, -3.734E-06)
°/km *W* sensitivities	(2.058E-04, 2.060E-04)	(-1.090E-03, -1.089E-03)	(4.597E-04, 4.599E-04)
°/km *IN* sensitivities	(4.022E-07, 3.876E-07)	(-4.035E-06, -3.941E-06)	(7.344E-07, 7.236E-07)

Table 6. Dual-valued sensitivity coefficients arising from ε_v variations at t_0 are presented with respect to nominal heliocentric J2KE elements at t_D.

t_0 Variations →	$v_1 \mp \varepsilon_v$	$v_2 \mp \varepsilon_v$	$v_3 \mp \varepsilon_v$
s/km *EC* sensitivities	(-6.441E-04, -6.440E-04)	(7.566E-04, 7.583E-04)	(-1.763E-04, -1.756E-04)
AU/km/s *QR* sensitivities	(8.813E-04, 8.813E-04)	(-2.596E-03, -2.599E-03)	(2.311E-04, 2.298E-04)
day/km/s *TP* sensitivities	(-7.037E-01, -7.032E-01)	(-3.316E+00, -3.316E+00)	(-2.184E-01, -2.186E-01)
°/km/s *OM* sensitivities	(1.755E-03, 1.751E-03)	(3.883E-02, 3.884E-02)	(2.790E-02, 2.790E-02)
°/km/s *W* sensitivities	(-6.033E-01, -6.028E-01)	(-3.799E+00, -3.799E+00)	(-2.198E-01, -2.202E-01)
°/km/s *IN* sensitivities	(1.958E-02, 1.958E-02)	(2.026E-02, 2.024E-02)	(7.130E-02, 7.130E-02)

Apollo 9 S-IVB-504 Reconstruction

Although crewed operations during Apollo 9 were confined to low Earth orbit, excess Saturn V launch vehicle performance permitted its S-IVB stage to be disposed in interplanetary space. Table 7 data recount pertinent mission events through disposal.

Table 7. The following Apollo 9 mission events led to S-IVB disposal.

GET (hhh:mm:ss)	1969 GMT	Event
000:00:00	03 Mar 16:00:00	Launch [12, p. 224]
000:11:15	03 Mar 16:11:15	Earth orbit insertion following S-IVB Burn #1: H_A = +186.57 km, H_P = +184.61 km [12, p. 230]
002:41:16	03 Mar 18:41:16	CSM separates from S-IVB [12, p. 230]
004:08:09	03 Mar 20:08:09	Mated CSM/LM is ejected from S-IVB [12, p. 230]
004:47:08	03 Mar 20:47:08	Intermediate orbit insertion following S-IVB Burn #2: H_A = +3095.77 km, H_P = +195.85 km [12, p. 230]
006:11:31	03 Mar 22:11:31	Escape orbit insertion following S-IVB Burn #3 [12, p. 231]: C_3 = +0.824712 km^2/s^2 [14, p. 4-14]
007:42:00	03 Mar 23:42:00	Approximate termination of all S-IVB propulsive accelerations [14, p. 4-7]
007:45:50	03 Mar 23:45:50	Final published S-IVB NAT elements and epoch t_0 [14, p. C-75]

Due to loss of pneumatic control, propulsive S-IVB propellant dumps planned to follow Burn #3 were never performed [12, p. 227]. Epoch t_0 S-IVB NAT elements [14, p. C-75] and corresponding nominal J2K Cartesian components are as follows.

Table 8. Nominal geocentric initial conditions for the Apollo 9 S-IVB EDTR are expressed as reported NAT elements [14, p. C-75] and as equivalent J2K Cartesian components.

Epoch t_0 = 03 Mar 1969 at 062/23:45:50.0 GMT	
NAT Elements	**J2K Components**
h = +14,087.332 nm	r_1 = +23,478.559086 km
ϕ = +25.9555°	r_2 = +17,297.941703 km
λ = -122.0914°	r_3 = +14,263.169924 km
s = 16,608.6 ft/s	v_1 =+2.091023077 km/s
γ = +59.34°	v_2 = +4.497024274 km/s
ψ = 112.66°	v_3 = +1.015524211 km/s

Very little independent trajectory data are available with which to verify nominal S-IVB EDTR from t_0 to t_D at 11.0 Mar 1969 GMT. Arguably the most critical such data known are reported S-IVB heliocentric orbit r_A = 148,678,656 km and r_P = 128,561,640 km [14, p. 4-15]. Figure 6 compares these reported apses with osculating values at hourly intervals during the nominal EDTR. As the S-IVB enters interplanetary space, Figure 6 indicates the degree to which reported apsis values are being approached asymptotically, a necessary condition for consistency.

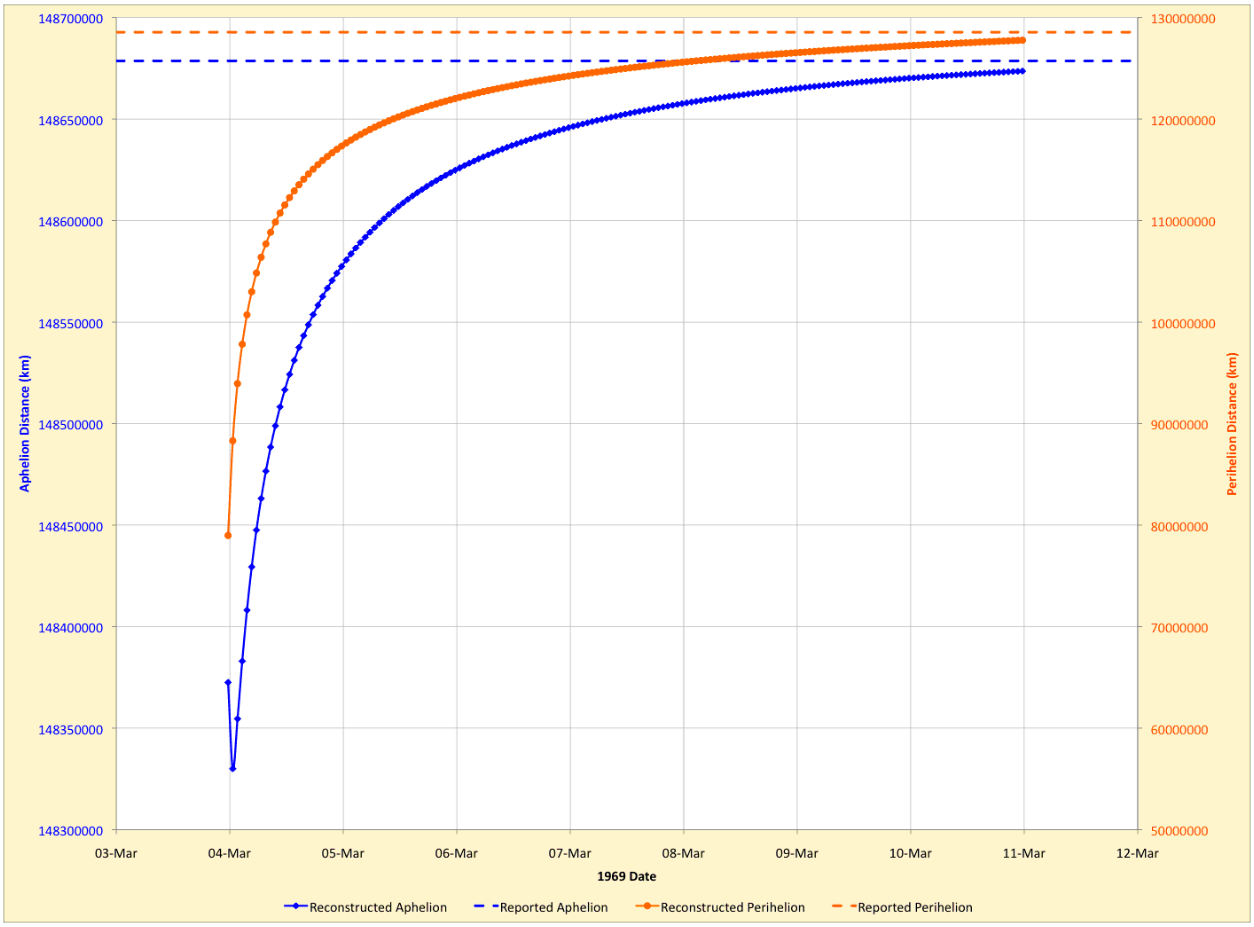

Figure 6. Apollo 9 S-IVB osculating aphelion (blue diamonds) and perihelion (orange dots) distances are plotted during nominal EDTR from 3 to 11 Mar 1969 GMT. Reported values for these apses [14, p. 4-15] are plotted as dashed lines of the corresponding color. As expected, each nominal apsis asymptotically approaches its reported value while the EDTR progresses toward interplanetary space.

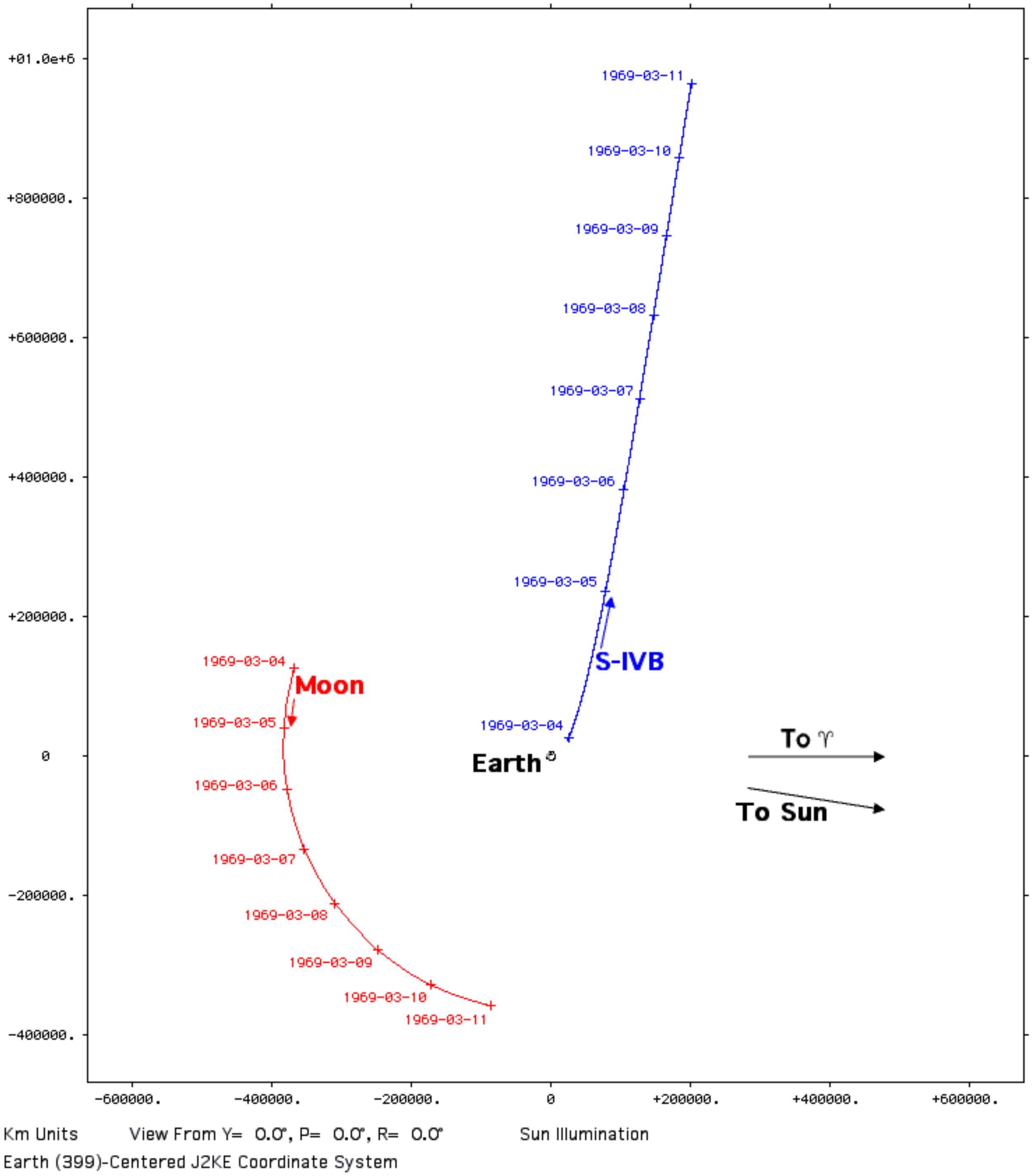

Figure 7. This geocentric inertial trajectory plot is viewed from the ecliptic north pole and illustrates Apollo 9 S-IVB nominal EDTR. The departure asymptote lies nearly opposite Earth's heliocentric motion as inferred from the Sun's direction. Time ticks are at even GMT dates and annotated in year-month-day format.

Table 9. Terminal geocentric position *r'* and velocity *v'* for the nominal Apollo 9 S-IVB EDTR are given with J2K Cartesian components.

Epoch t_D = 11.0 Mar 1969 GMT
r_1' = +201,219.003246 km
r_2' = +1,031,661.103409 km
r_3' = +44,202.457597 km
v_1' = +0.198229807 km/s
v_2' = +1.327208257 km/s
v_3' = +0.014759432 km/s

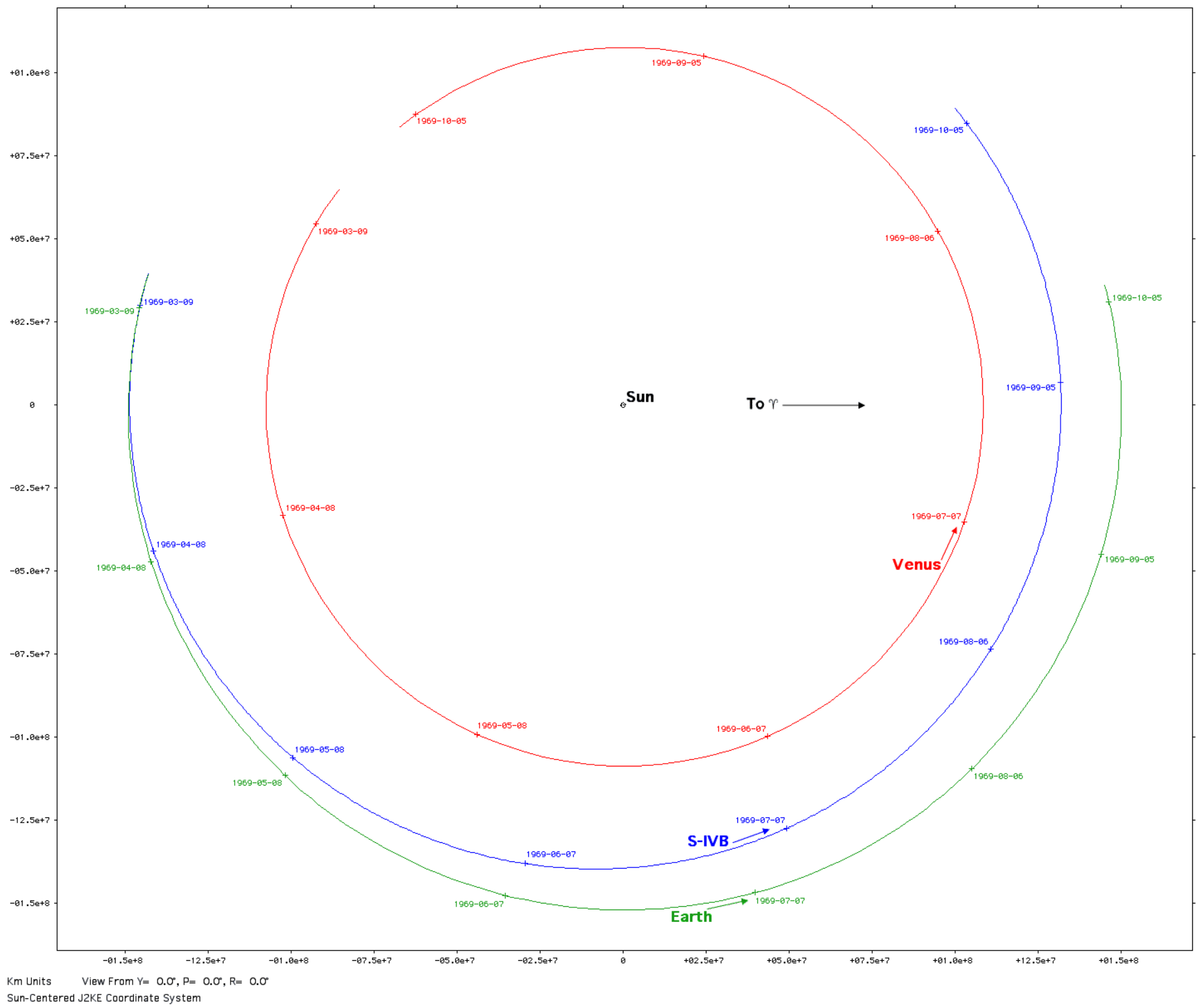

Figure 8. ***Horizons*** **prediction of Apollo 9 S-IVB inertial heliocentric motion from Table 9 data is plotted with corresponding Earth and Venus motion for the first seven months following S-IVB disposal. Time ticks are at 30-day intervals and annotated in year-month-day format.**

Total uncertainty associated with Table 8 Apollo 9 S-IVB ***r*** and ***v*** at t_0 is estimated to be $\varepsilon_r = \pm 1$ km in each position component and $\varepsilon_v = \pm 0.003$ km/s in each velocity component [14, p. 3-8]. Dual-valued sensitivity coefficients arising from ε_r variations at t_0 (m_{ij} with $i = 1 \rightarrow 6$; $j = 1 \rightarrow 3$) appear in Table 10, and dual-valued sensitivity coefficients arising from ε_v variations at t_0 (m_{ij} with $i = 1 \rightarrow 6$; $j = 4 \rightarrow 6$) appear in Table 11.

Table 10. Dual-valued sensitivity coefficients arising from ε_r variations at t_0 are presented with respect to nominal heliocentric J2KE elements at t_D.

t_0 Variations →	$r_1 \mp \varepsilon_r$	$r_2 \mp \varepsilon_r$	$r_3 \mp \varepsilon_r$
km^{-1} *EC* sensitivities	(1.122E-05, 1.120E-05)	(8.523E-06, 8.503E-06)	(6.128E-06, 6.128E-06)
AU/km *QR* sensitivities	(-1.951E-05, -1.948E-05)	(-1.508E-05, -1.504E-05)	(-1.080E-05, -1.080E-05)
day/km *TP* sensitivities	(7.053E-04, 7.036E-04)	(-2.671E-04, -2.689E-04)	(-5.583E-05, -5.568E-05)
°/km *OM* sensitivities	(2.912E-04, 2.899E-04)	(2.122E-04, 2.109E-04)	(2.051E-04, 2.050E-04)
°/km *W* sensitivities	(-2.185E-03, -2.180E-03)	(-2.486E-03, -2.482E-03)	(-1.698E-03, -1.697E-03)
°/km *IN* sensitivities	(8.424E-05, 8.406E-05)	(4.598E-05, 4.581E-05)	(1.014E-04, 1.014E-04)

Table 11. Dual-valued sensitivity coefficients arising from ε_v variations at t_0 are presented with respect to nominal heliocentric J2KE elements at t_D.

t_0 Variations →	$v_1 \mp \varepsilon_v$	$v_2 \mp \varepsilon_v$	$v_3 \mp \varepsilon_v$
s/km *EC* sensitivities	(8.562E-02, 8.554E-02)	(1.792E-01, 1.784E-01)	(5.119E-02, 5.126E-02)
AU/km/s *QR* sensitivities	(-1.531E-01, -1.528E-01)	(-3.126E-01, -3.109E-01)	(-8.928E-02, -8.937E-02)
day/km/s *TP* sensitivities	(-7.138E+00, -7.022E+00)	(8.578E+00, 8.931E+00)	(2.341E+00, 2.378E+00)
°/km/s *OM* sensitivities	(2.274E+00, 2.256E+00)	(4.671E+00, 4.583E+00)	(1.376E+00, 1.375E+00)
°/km/s *W* sensitivities	(-2.979E+01, -2.961E+01)	(-3.771E+01, -3.702E+01)	(-1.093E+01, -1.090E+01)
°/km/s *IN* sensitivities	(7.082E-01, 7.063E-01)	(1.772E+00, 1.763E+00)	(-3.847E-01, -3.862E-01)

Apollo 10 S-IVB-505 Reconstruction

Using residual propellant dumps following TLI and CSM/LM ejection, the Apollo 10 S-IVB approached the Moon over its trailing hemisphere and obtained a gravity assist leading to disposal in interplanetary space. Table 12 data recount pertinent mission events through disposal.

Table 12. The following Apollo 10 mission events led to S-IVB disposal.

GET (hhh:mm:ss)	1969 GMT	Event
000:00:00	18 May 16:49:00	Launch [12, p. 256]
000:11:54	18 May 17:00:54	Earth orbit insertion following S-IVB Burn #1: H_A = +185.79 km, H_P = +184.66 km [12, p. 259]
002:39:21	18 May 19:28:21	TLI following S-IVB Burn #2 [12, p. 275]
003:02:42	18 May 19:51:42	CSM separation from S-IVB [12, p. 275] and epoch t_0 at final published S-IVB NAT elements [15, p. 4-7]
003:56:26	18 May 20:45:26	Mated CSM/LM is ejected from S-IVB [12, p. 275]
004:45:36	18 May 21:34:36	S-IVB post-TLI propulsive accelerations are initiated [12, p. 275]
004:57:00	18 May 21:46:00	Approximate midpoint of post-TLI S-IVB propulsive accelerations and epoch t_1
005:29:05	18 May 22:18:05	S-IVB post-TLI propulsive accelerations are terminated [12, p. 276]
078:51:04	21 May 23:40:04	S-IVB pericynthion passage and epoch t_2: H_P = +3112 km [15, p. 6-1]

Table 13. Nominal geocentric initial conditions for the Apollo 10 S-IVB EDTR are expressed as reported NAT elements [15, p. 4-7] and as equivalent J2K Cartesian components.

Epoch t_0 = 18 May 1969 at 138/19:51:42.4 GMT	
NAT Elements	**J2K Components**
h = +3502.62 nm	r_1 = +9712.937072 km
ϕ = +22.967°	r_2 = +6763.907212 km
λ = -139.826°	r_3 = +5033.260149 km
s = 25,548.72 ft/s	v_1 = +0.430034019 km/s
γ = +43.928°	v_2 = +6.617017492 km/s
ψ = 67.467°	v_3 = +4.083063871 km/s

Table 13 nominal $\boldsymbol{r}$ and $\boldsymbol{v}$ are coasted from t_0 to t_1, where geocentric position and t_1 serve as initial boundary conditions in a perturbed Lambert problem whose final boundary conditions are t_2, selenocentric H_P = +3112 km [15, p. 6-1], and selenocentric λ = +66° inferred from t_2 mapped onto a lunar flyby trajectory plot [15, p. 6-5]. The plot's annotated "TOWARD EARTH" direction is assumed to also point at selenocentric $\lambda = 0$ while performing this mapping. Because the plot is two-dimensional and lies near the lunar equatorial plane, selenocentric ϕ at t_2 cannot be inferred from it.

A solution to the t_1/t_2 Lambert problem is therefore sought such that deviation from final position is less than 0.001 km as selenocentric ϕ at t_2 is iterated to achieve the selenocentric γ closest to zero at t_2. Results of this iteration appear in Table 14, where $|\boldsymbol{\Delta v}|$ is the magnitude of a velocity increment computed at t_1 as the vector difference between the perturbed Lambert solution's initial velocity minus velocity in the nominal EDTR as coasted from Table 13 initial conditions to t_1.

Table 14. Results from evaluating multiple perturbed Lambert solutions over the t_1/t_2 arc are recorded as selenocentric ϕ at t_2 is iterated. Selenocentric h = +3112 km and λ = +66° are held constant at their reported t_2 values during this process. The ϕ = +12° solution is adopted by the EDTR because its selenocentric γ is nearest to zero, a necessary and sufficient condition for pericynthion in a lunar flyby.

ϕ (deg)	$\lvert\Delta\boldsymbol{v}\rvert$ (km/s)	γ (deg)
+7	0.043831	-0.138
+8	0.043991	-0.112
+11	0.044532	-0.072
+12	0.044732	-0.071
+13	0.044941	-0.077
+20	0.046619	-0.294

The reported longitudinal body-fixed component of all S-IVB propulsive accelerations in the t_1 time frame is 0.0442 km/s [15, p. 6-2]. The Table 14 $|\Delta\boldsymbol{v}|$ = 0.044732 km/s associated with ϕ = +12° is corroborated by the reported acceleration component, whose value must be slightly smaller than a credible $|\Delta\boldsymbol{v}|$ defined to encompass the entire velocity increment at t_1. This "best fit" Lambert solution is associated with $\Delta\boldsymbol{v} = [+0.03963277, -0.02010951, +0.00507877]^T$ km/s expressed in J2K Cartesian components at t_1. The t_1 impulse leading to pericynthion at selenocentric ϕ = +12° is incorporated as an event in the Apollo 10 S-IVB nominal EDTR.

Reported S-IVB heliocentric orbit aphelion distance r_A = 152,160,000 km and perihelion distance r_P = 135,810,000 km [15, p. 6-8]. Figure 9 compares these reported apses with osculating values at hourly intervals during the nominal EDTR. As the S-IVB enters interplanetary space, Figure 9 indicates the degree to which reported apsis values are being approached asymptotically, a necessary condition for consistency.

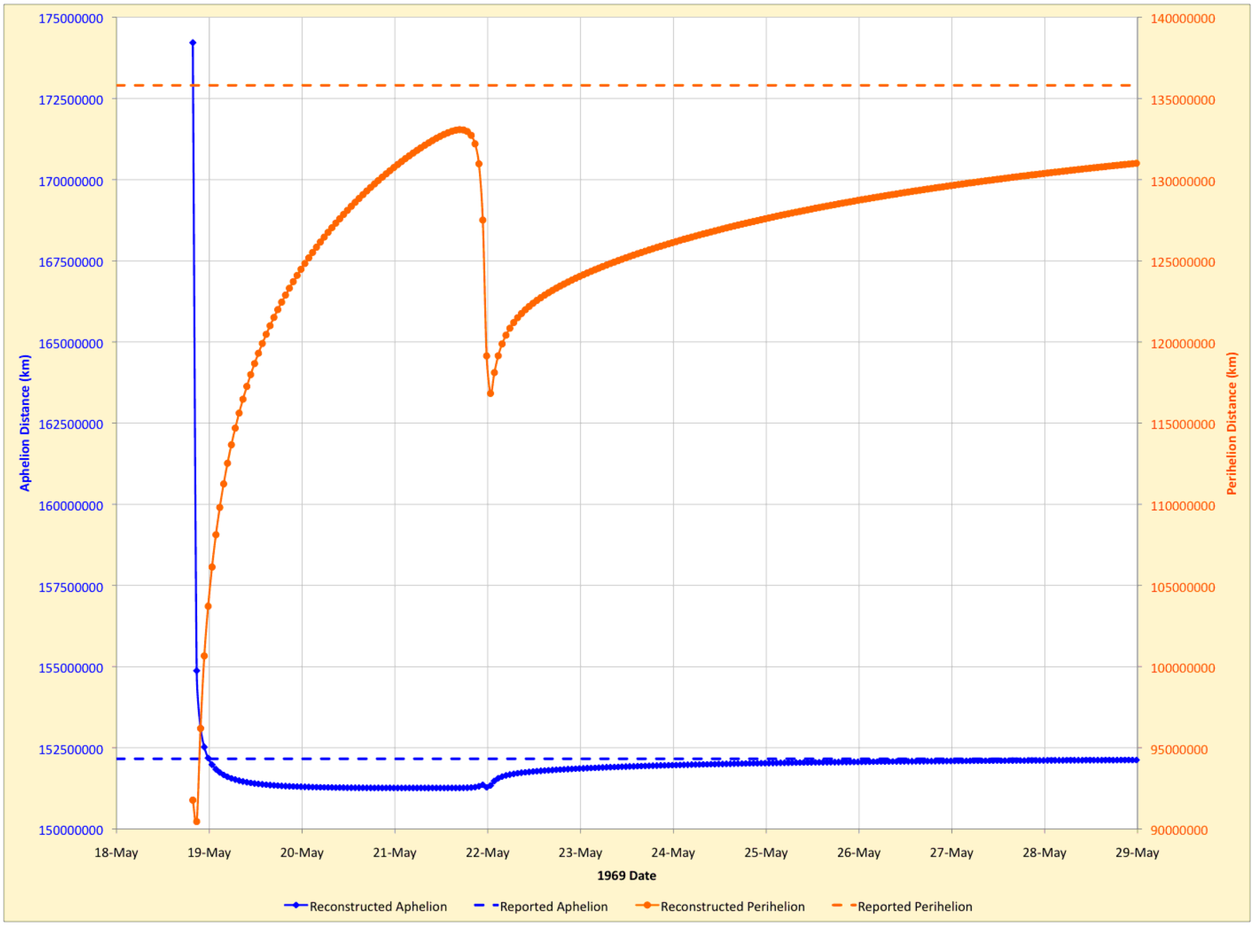

Figure 9. Apollo 10 S-IVB osculating aphelion (blue diamonds) and perihelion (orange dots) distances are plotted during nominal EDTR from 18 to 29 May 1969 GMT. Reported values for these apses [15, p. 6-8] are plotted as dashed lines of the corresponding color. As expected, each nominal apsis asymptotically approaches its reported value while the EDTR progresses toward interplanetary space. Rapidly varying EDTR apses on 21-22 May reflect the effects of lunar encounter.

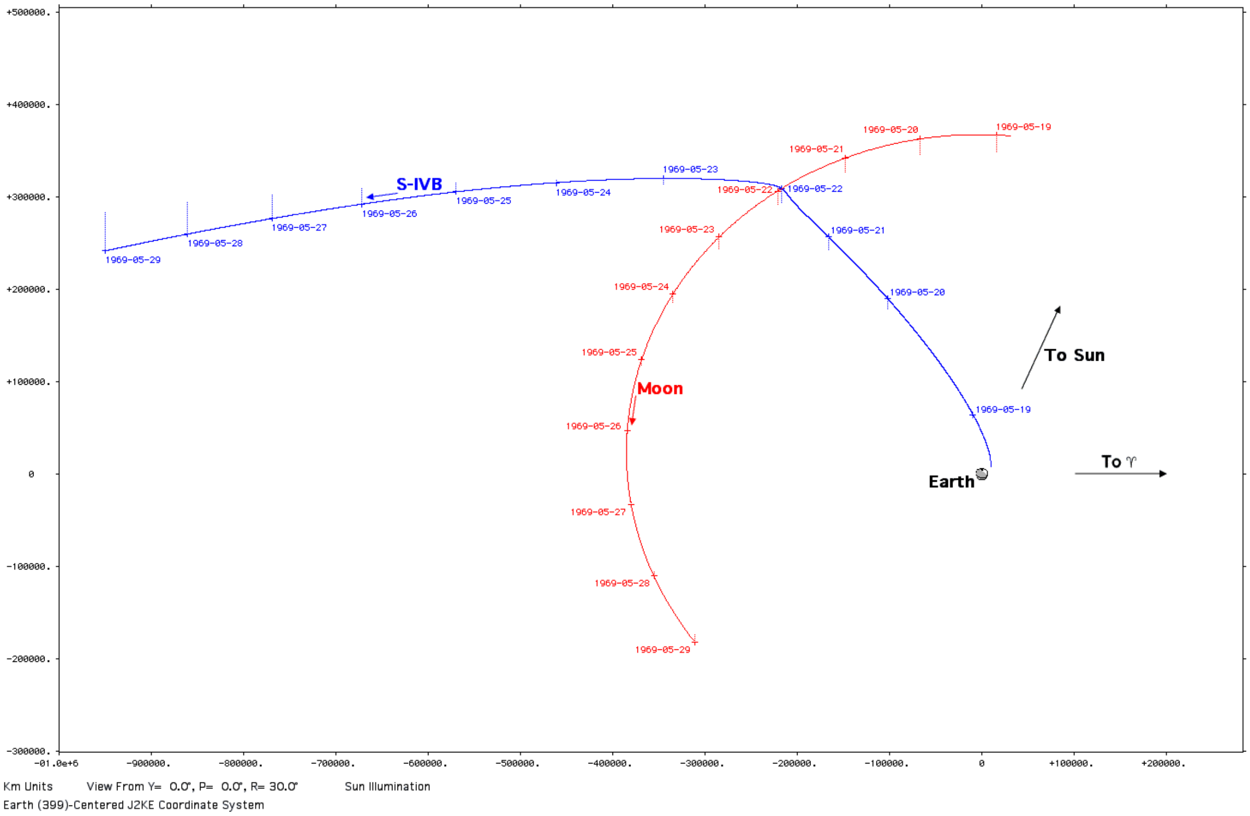

Figure 10. This geocentric inertial trajectory plot is viewed from ecliptic longitude 270°; latitude +60° and illustrates Apollo 10 S-IVB nominal EDTR. The departure asymptote lies nearly opposite Earth's heliocentric motion as inferred from the Sun's direction. Time ticks are at even GMT dates and annotated in year-month-day format. Dotted lines are projections onto the ecliptic plane.

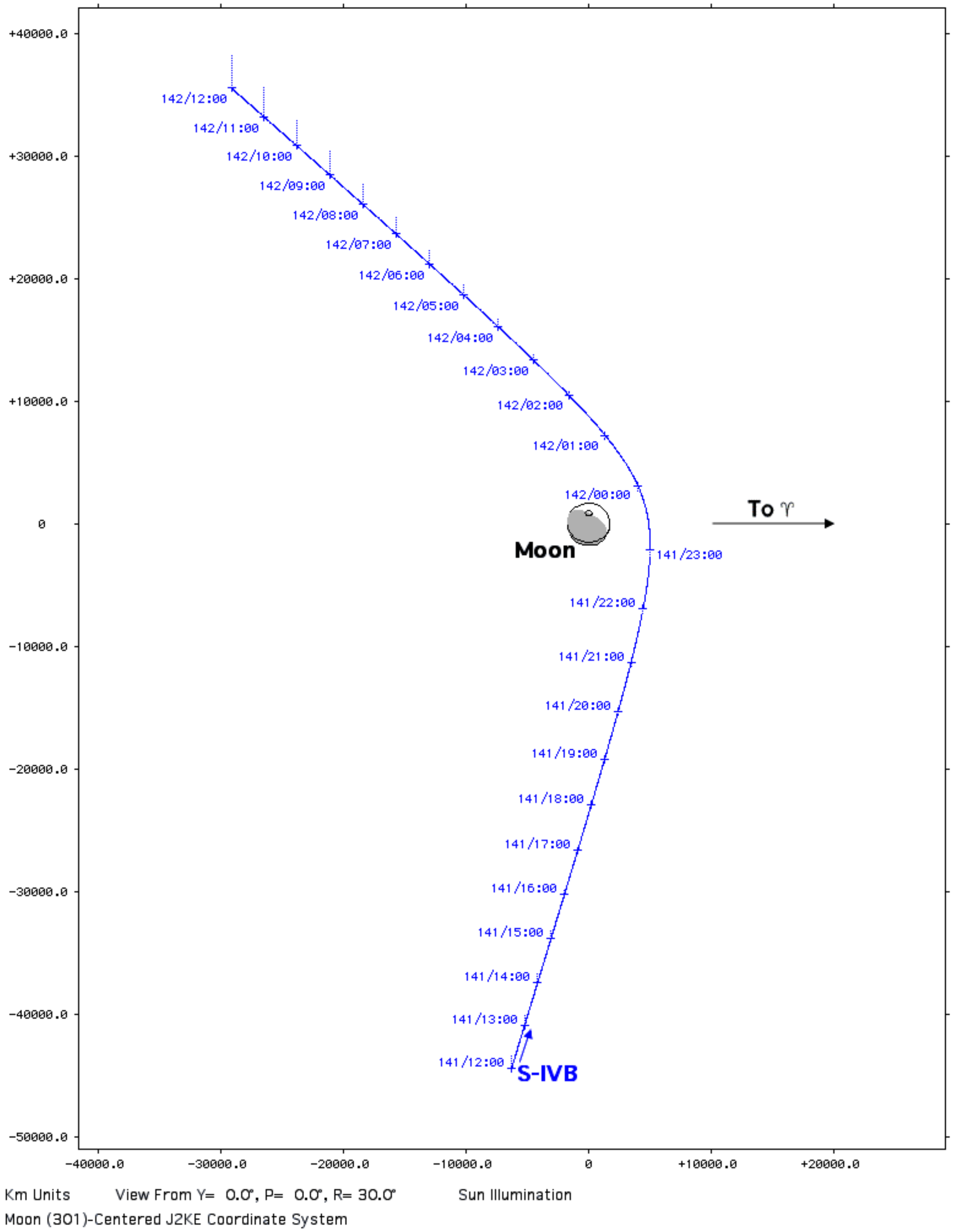

Figure 11. This inertial trajectory plot illustrates nominal Apollo 10 S-IVB EDTR selenocentric motion during 21-22 May 1969 GMT and is viewed from the same perspective as Figure 10 (ecliptic longitude 270°; latitude +60°). The Moon's shaded hemisphere is its nightside. Time tick annotations are at one-hour intervals in day-of-year/hh:mm format. Dotted lines are projections onto the ecliptic plane.

Table 15. Terminal geocentric position *r'* and velocity *v'* for the nominal Apollo 10 S-IVB EDTR are given with J2K Cartesian components.

Epoch t_D = 29.0 May 1969 GMT
r_1' = -949,923.267040 km
r_2' = +332,974.109050 km
r_3' = +53,977.763111 km
v_1' = -1.007974142 km/s
v_2' = -0.062381644 km/s
v_3' = -0.219526330 km/s

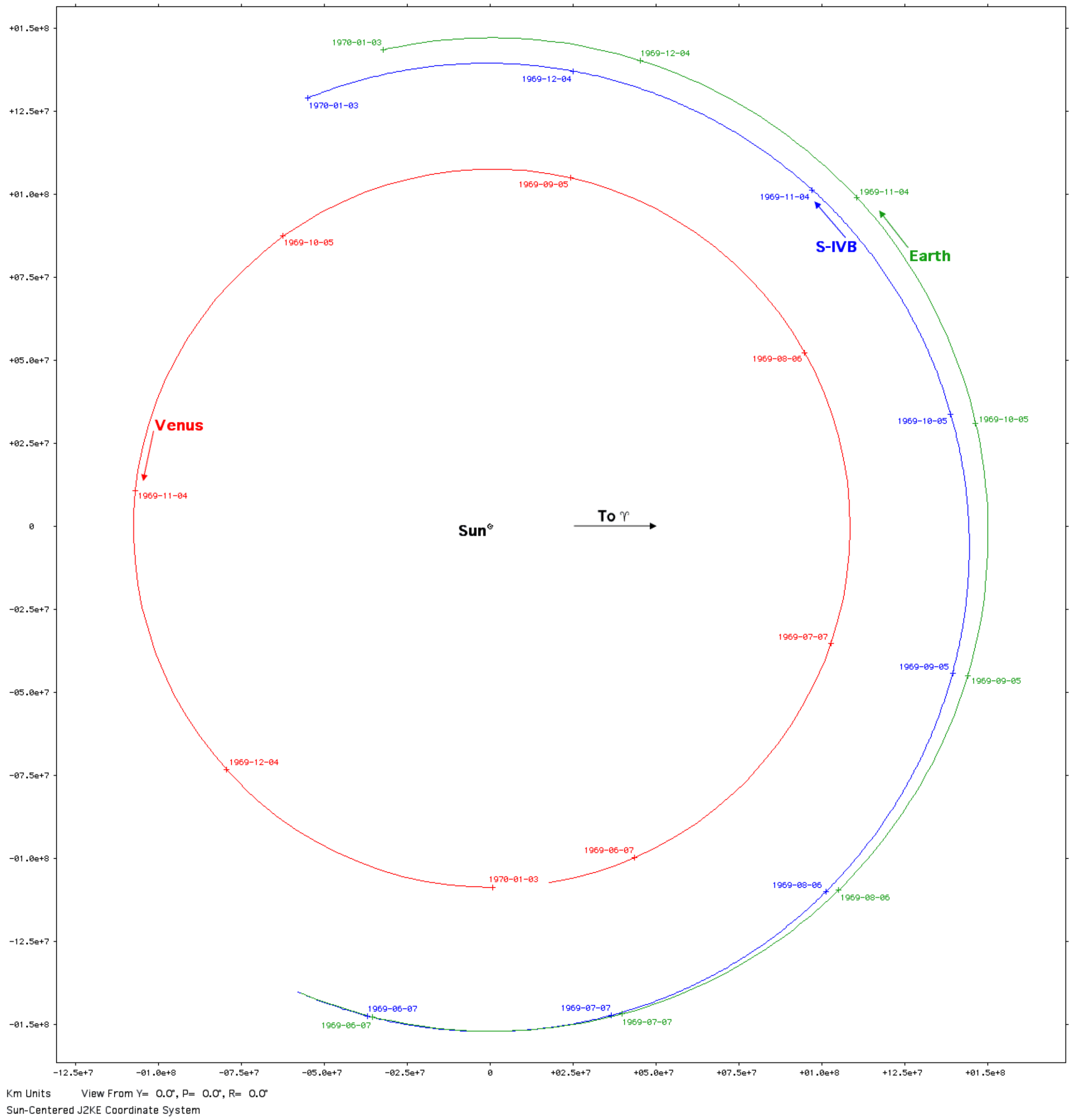

Figure 12. ***Horizons*** **prediction of Apollo 10 S-IVB inertial heliocentric motion from Table 15 data is plotted with corresponding Earth and Venus motion for the first seven months following S-IVB disposal. Time ticks are at 30-day intervals and annotated in year-month-day format.**

Reported S-IVB trajectory error analysis ends *during* the S-IVB Burn #2 interval preceding TLI. At that point in the Apollo 10 mission, estimated $\varepsilon_r = \pm 0.5$ km in each position component and estimated $\varepsilon_v = \pm 0.001$ km/s in each velocity component [15, p. 3-7]. Because TLI occurred over 23 min before EDTR initialization at t_0, reported trajectory uncertainties are likely smaller during Burn #2 than would be appropriate for computing post-TLI EDTR sensitivity coefficients.

Reported error analyses, cited earlier in this paper for the previous two Saturn V launches on missions Apollo 8 and Apollo 9, estimate $\varepsilon_r = \pm 1$ km in each position component and $\varepsilon_v = \pm 0.003$ km/s in each velocity component during those post-TLI trajectories. Consequently, the Apollo 10 S-IVB EDTR sensitivity analysis adopts these larger, more conservative values for ε_r and ε_v. Dual-valued sensitivity coefficients arising from ε_r variations at t_0 (m_{ij} with $i = 1 \rightarrow 6; j = 1 \rightarrow 3$) appear in Table 16, and dual-valued sensitivity coefficients arising from ε_v variations at t_0 (m_{ij} with $i = 1 \rightarrow 6; j = 4 \rightarrow 6$) appear in Table 17.

Table 16. Dual-valued sensitivity coefficients arising from ε_r variations at t_0 are presented with respect to nominal heliocentric J2KE elements at t_D.

t_0 Variations →	$r_1 \mp \varepsilon_r$	$r_2 \mp \varepsilon_r$	$r_3 \mp \varepsilon_r$
km^{-1} *EC* sensitivities	(-5.748E-08, -5.750E-08)	(-6.767E-08, -6.773E-08)	(-4.442E-08, -4.445E-08)
AU/km *QR* sensitivities	(3.126E-07, 3.127E-07)	(3.543E-07, 3.544E-07)	(2.418E-07, 2.418E-07)
day/km *TP* sensitivities	(4.257E-04, 4.256E-04)	(4.732E-04, 4.731E-04)	(3.293E-04, 3.293E-04)
°/km *OM* sensitivities	(-1.336E-05, -1.338E-05)	(-1.615E-05, -1.618E-05)	(-7.728E-06, -7.742E-06)
°/km *W* sensitivities	(4.735E-04, 4.736E-04)	(5.286E-04, 5.286E-04)	(3.637E-04, 3.637E-04)
°/km *IN* sensitivities	(2.085E-06, 2.088E-06)	(2.567E-06, 2.572E-06)	(1.092E-06, 1.095E-06)

Table 17. Dual-valued sensitivity coefficients arising from ε_v variations at t_0 are presented with respect to nominal heliocentric J2KE elements at t_D.

t_0 Variations →	$v_1 \mp \varepsilon_v$	$v_2 \mp \varepsilon_v$	$v_3 \mp \varepsilon_v$
s/km *EC* sensitivities	(2.467E-04, 2.462E-04)	(-3.167E-04, -3.169E-04)	(-4.146E-04, -4.144E-04)
AU/km/s *QR* sensitivities	(3.131E-04, 3.142E-04)	(1.036E-03, 1.036E-03)	(1.063E-03, 1.063E-03)
day/km/s *TP* sensitivities	(1.536E+00, 1.537E+00)	(9.501E-01, 9.498E-01)	(6.481E-01, 6.480E-01)
°/km/s *OM* sensitivities	(-1.561E-02, -1.595E-02)	(1.283E-01, 1.284E-01)	(-2.885E-01, -2.882E-01)
°/km/s *W* sensitivities	(1.569E+00, 1.569E+00)	(9.435E-01, 9.431E-01)	(1.067E+00, 1.066E+00)
°/km/s *IN* sensitivities	(2.005E-03, 2.079E-03)	(-2.731E-02, -2.730E-02)	(5.591E-02, 5.590E-02)

Apollo 10 LM-4 *Snoopy* Ascent Stage Reconstruction

The Apollo 10 mission tested LM systems in lunar orbit for the first time, but no landing on the Moon was planned or attempted. During autonomous lunar orbit operations, the LM jettisoned its descent stage at a selenocentric $h = +58.2$ km [12, p. 262]. Because the crewed ascent stage was not launched from the Moon's surface, CSM docking (see Figure 13) was achieved with considerable propellant still aboard the LM. Following docking and crew transfer to the CSM for Earth return, the LM was jettisoned and its surplus propellant expended in ground-commanded separation and depletion burns ultimately departing the Moon and Earth for interplanetary space. Table 18 recounts pertinent mission events leading to LM disposal.

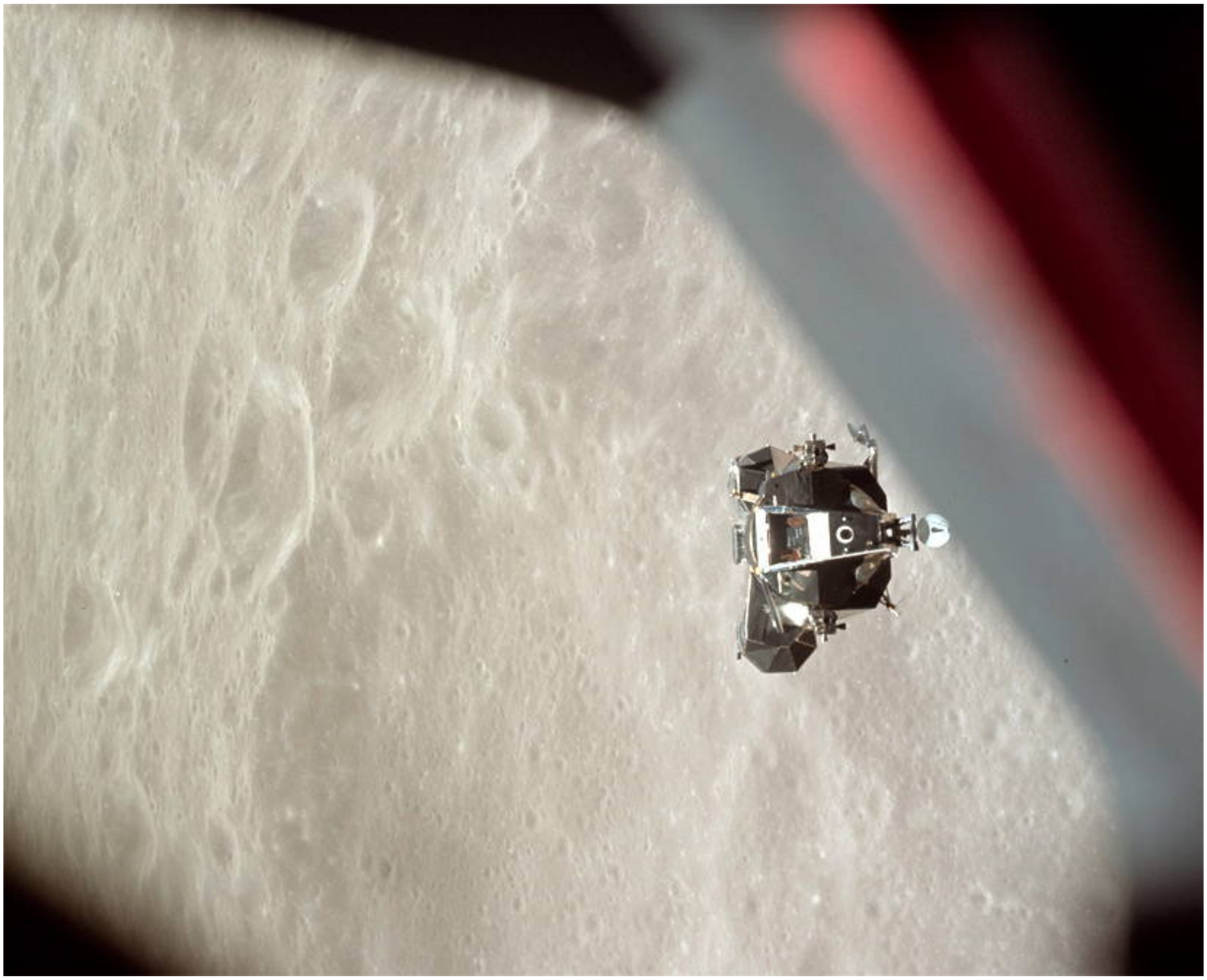

Figure 13. This NASA image obtained from the CSM shows the Apollo 10 LM ascent stage preparing to dock following autonomous crewed operations in lunar orbit.

Table 18. The following Apollo 10 mission events led to LM disposal.

GET (hhh:mm:ss)	1969 GMT	Event
000:00:00	18 May 16:49:00	Launch [12, p. 256]
076:01:50	21 May 20:50:50	CSM/LM lunar orbit insertion: H_A = +314.8 km, H_P = +111.5 km [12, p. 262]
080:25:22	22 May 01:14:22	CSM/LM orbit circularization: H_A = +113.0 km, H_P = +109.6 km [12, p. 262]
098:11:57	22 May 19:00:57	CSM/LM undocking [12, p. 262]
100:41:43	22 May 21:30:43	LM closest approach to the Moon: h = +14.4 km [12, p. 262]
102:45:17	22 May 23:34:17	LM descent stage jettison: h = +58.2 km [12, p. 262]
106:22:02	23 May 03:11:02	CSM/LM docking [12, p. 263]
108:24:36	23 May 05:13:36	LM jettison [12, p. 262]
108:43:30	23 May 05:32:30	LM separation burn cutoff and epoch t_A: H_A = +118.5 km, H_P = +104.3 km [12, p. 263]
108:52:05	23 May 05:41:05	LM propellant depletion burn ignition and epoch t_B [12, p. 263]
108:56:14	23 May 05:45:14	LM propellant depletion burn cutoff and epoch t_0 [12, p. 263]

The Apollo 10 LM's EDTR requires special consideration because it is the only one in this study to require selenocentric NAT elements. Experience with previous NAT-based reconstructions has shown selenocentric ψ values may reflect either of two differing reference headings in the local horizontal plane [17, p. 41]. One reference is the direction from the Earth's center to its true north rotational pole projected onto the selenocentric local horizontal plane (termed the geocentric pole reference), and the other reference is the direction from the Moon's center to its true north rotational pole projected onto this plane (termed the selenocentric pole reference).

Consequently, pre-disposal selenocentric NAT element sets at epochs t_A and t_B [16, p. 6-9] are used to define an 8.6-min coasted arc in lunar orbit as a test of correct NAT interpretation. Because selenocentric position inferred from NAT elements is independent of ψ, positions inferred at t_A and t_B define a perturbed Lambert boundary value problem whose solution is also unaffected by ψ at either epoch. A necessary and sufficient condition for correct NAT elements interpretation is a Lambert solution trajectory whose corresponding velocities are consistent with those inferred from NAT elements at t_A or t_B.

The t_A/t_B Lambert solution has t_A selenocentric velocity with ψ = 269.050°, matching the reported NAT value at that epoch. It is therefore assumed the ψ from NAT elements at epoch t_0 reflects a selenocentric pole reference. This assumption is further supported by other selenocentric NAT element sets [16, p. 6-9] during Apollo 10's lunar orbit phase. None of the associated ϕ values departs from the Moon's equator by more than 1.12°. Indeed, the t_A/t_B Lambert solution has selenocentric inclination of 178.838°. But assuming a geocentric pole reference with the ψ value at t_A converts associated NAT elements at that epoch into an orbit with selenocentric inclination 159.704°. Selenocentric ϕ values approaching 20° in magnitude would be expected in such an orbit. Table 19 documents conversion of selenocentric LM NAT elements under the selenocentric pole reference assumption for ψ.

Table 19. Nominal selenocentric initial conditions for the Apollo 10 LM EDTR are expressed as reported NAT elements [16, p. 6-9] and as equivalent J2K Cartesian components.

Epoch t_0 = 23 May 1969 at 143/05:45:14.5 GMT	
NAT Elements	**J2K Components**
h = +89.7 nm	r_1 = +1037.390877 km
ϕ = +0.44°	r_2 = -1486.966437 km
λ = -20.22°	r_3 = -582.044542 km
s = 9056.4 ft/s	v_1 = -1.963730586 km/s
γ = +11.63°	v_2 = -1.787849755 km/s
ψ = 269.19°	v_3 = -0.753068632 km/s

No further trajectory-related events or corroborating data are reported for the LM after t_0. Consequently, its EDTR is a simple coast of initial conditions from Table 19.

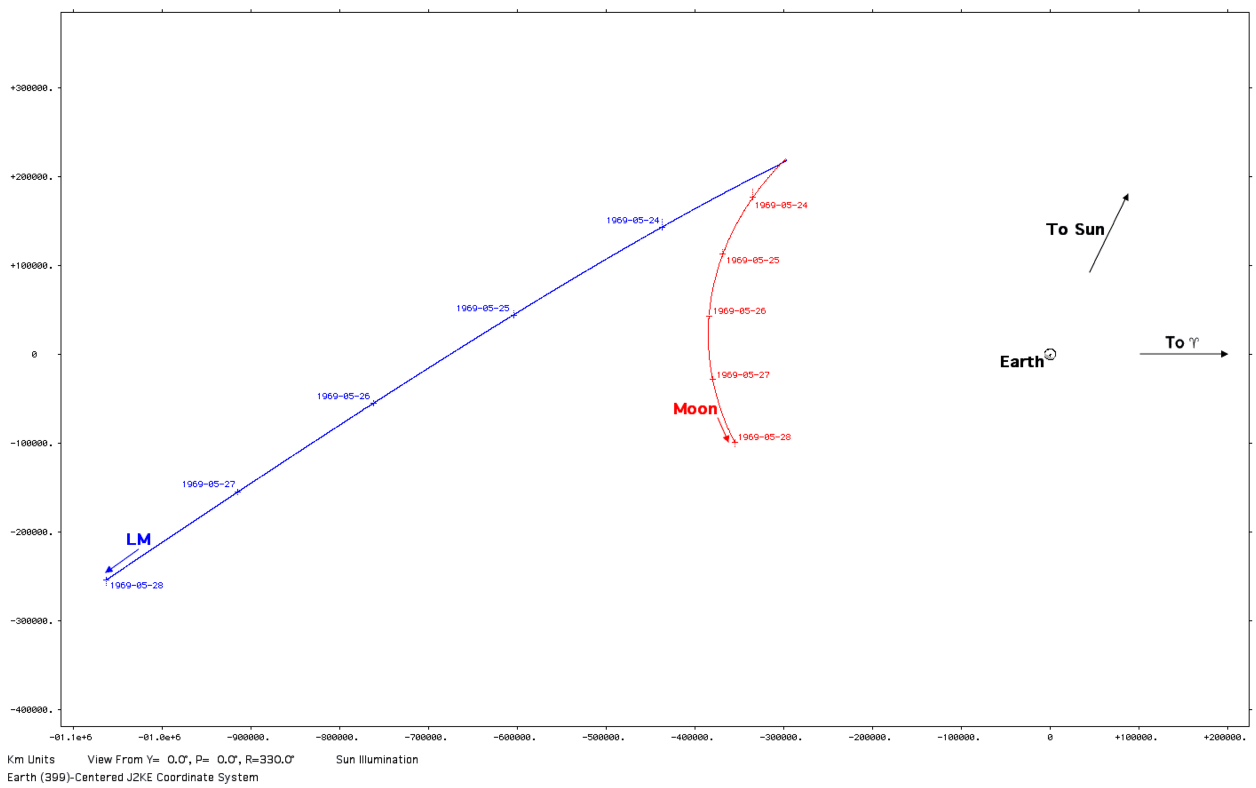

Figure 14. This geocentric inertial trajectory plot is viewed from ecliptic longitude 90°; latitude +60° and illustrates Apollo 10 LM nominal EDTR. Time ticks are at even GMT dates and annotated in year-month-day format. Dotted lines are projections onto the ecliptic plane.

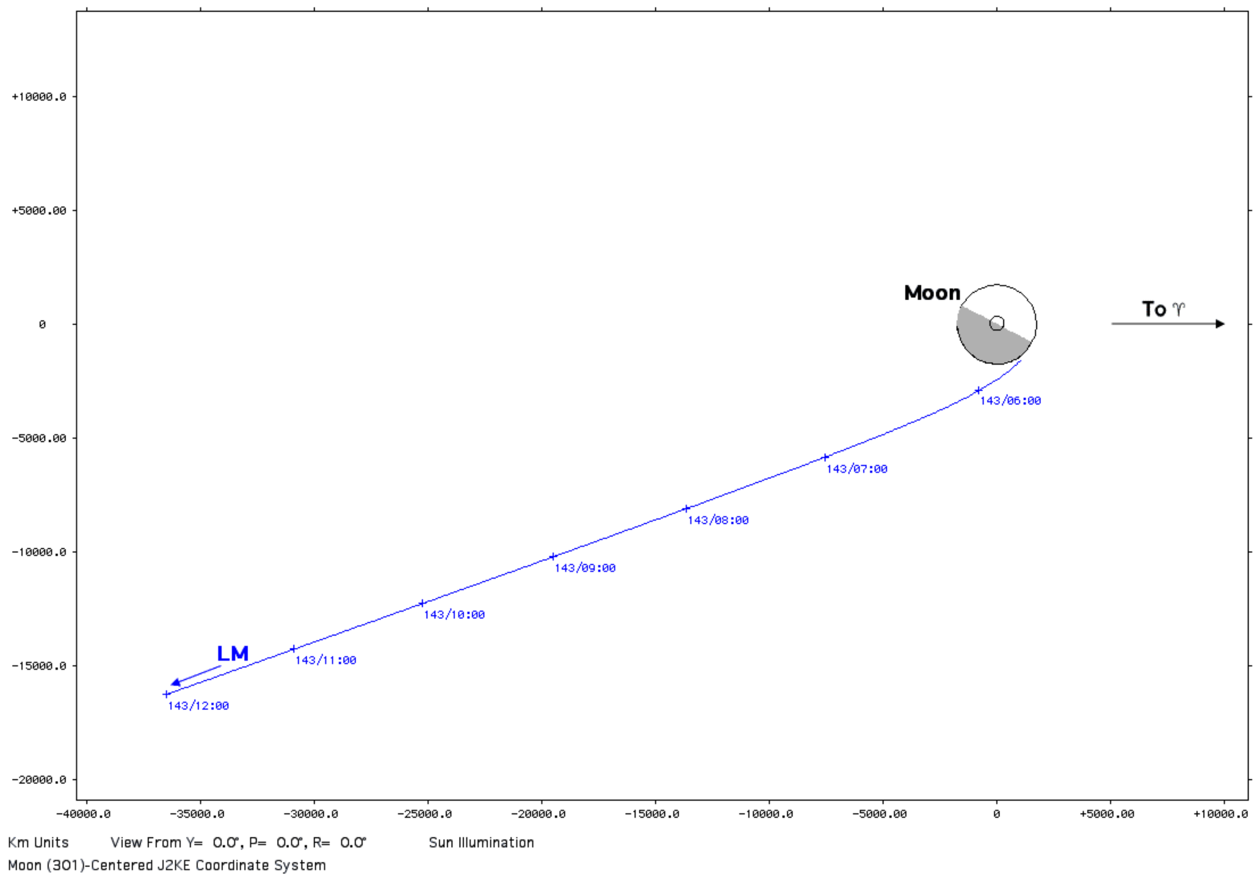

Figure 15. This inertial trajectory plot illustrates nominal Apollo 10 LM EDTR selenocentric motion during its initial 6 hrs on 23 May 1969 GMT and is viewed from ecliptic latitude +90°. The Moon's shaded hemisphere is its nightside. Time tick annotations are at one-hour intervals in day-of-year/hh:mm format.

Table 20. Terminal geocentric position *r'* and velocity *v'* for the nominal Apollo 10 LM EDTR are given with J2K Cartesian components.

Epoch t_D = 28.0 May 1969 GMT
r_1' = -1,063,397.768621 km
r_2' = -271,071.472475 km
r_3' = -131,364.666591 km
v_1' = -1.701807819 km/s
v_2' = -1.228163812 km/s
v_3' = -0.628508734 km/s

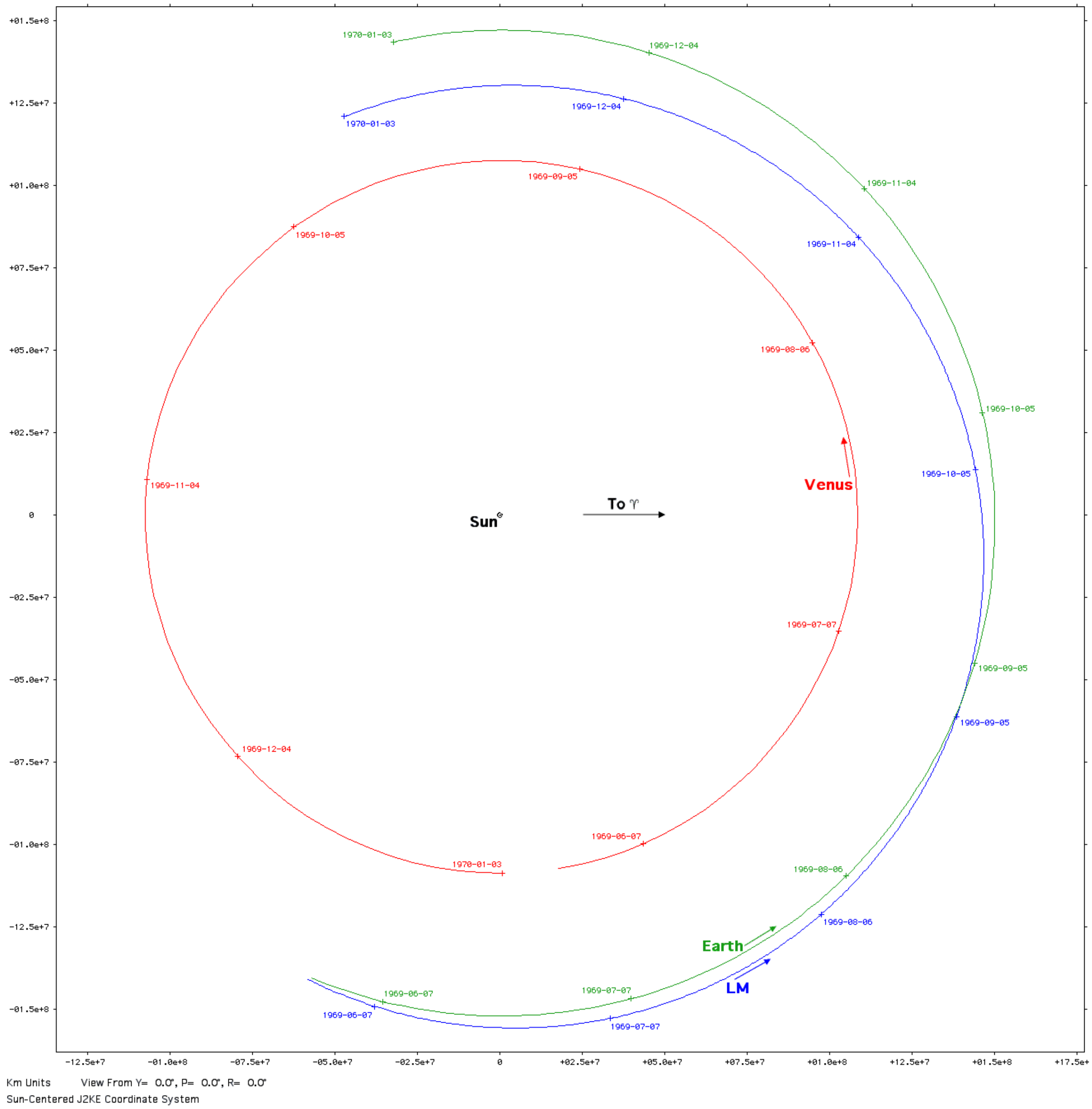

Figure 16. *Horizons* prediction of Apollo 10 LM inertial heliocentric motion from Table 20 data is plotted with corresponding Earth and Venus motion for the first seven months following LM disposal. Time ticks are at 30-day intervals and annotated in year-month-day format.

Reported trajectory uncertainty analysis during the lunar orbit phase of the Apollo 10 mission is expressed as downtrack, crosstrack, and radial "position errors, ft/rev" [16, p. 6-6]. Each of these error components is adopted as the corresponding component of selenocentric position uncertainty ε_r at t_0 for LM EDTR sensitivity analysis. Corresponding velocity error components are inferred using a coasted baseline trajectory initialized with the perturbed Lambert solution at t_A. A perturbed trajectory is identically initialized, but it incorporates an impulsive downtrack, crosstrack, or radial Δv 27.5 min after t_A on 23 May 1969 at 143/06:00 GMT. Initial conditions for the baseline and perturbed trajectories are presented in Table 21.

Table 21. Initial selenocentric position *r* and velocity *v* for the baseline and perturbed Apollo 10 LM trajectories are given with J2K Cartesian components. These trajectories support computation of inferred velocity uncertainties in the t_0 time frame, but *r* and *v* are also the reconstructed LM state vector following its jettison and separation from the CSM. The LM propellant depletion burn leading to disposal in interplanetary space began 8.6 min after t_A.

Epoch t_A = 23 May 1969 at 05:32:29.9 GMT
r_1 = +1790.279315 km
r_2 = -420.145432 km
r_3 = -146.727825 km
v_1 = -0.388293257 km/s
v_2 = -1.460636609 km/s
v_3 = -0.615580375 km/s

A given Δv component achieving the corresponding ε_r component as a local maximum in position deviation magnitude of the perturbed trajectory with respect to the baseline trajectory is adopted as the corresponding component of selenocentric velocity uncertainty ε_v at t_0 for LM EDTR sensitivity analysis. To elaborate, a purely downtrack Δv is iterated to produce a downtrack position deviation from the baseline trajectory equal in magnitude to the adopted downtrack position uncertainty. This condition occurs about an orbit after the impulse, and the associated Δv becomes the downtrack component of ε_v. Similarly, a purely crosstrack Δv is iterated to produce a crosstrack position deviation from the baseline trajectory equal in magnitude to the adopted crosstrack position uncertainty. This condition occurs about a quarter orbit after the impulse, and the associated Δv becomes the crosstrack component of ε_v. Finally, a purely radial Δv is iterated to produce a radial position deviation from the baseline trajectory equal in magnitude to the adopted radial position uncertainty. This condition also occurs about a quarter orbit after the impulse, and the associated Δv becomes the radial component of ε_v. Table 22 summarizes all LM uncertainties to be used in the EDTR sensitivity analysis, including results of these iterations.

Table 22. Position and velocity uncertainties adopted for Apollo 10 LM EDTR sensitivity analysis are directionally dependent (other EDTR uncertainties in this study are spherically symmetric). Components of position uncertainty are obtained by assuming reported position error after one lunar orbit [16, p. 6-6] is applicable at t_0. Velocity uncertainty components are inferred from the reported position error growth rate.

Component	ε_r (km)	ε_v (km/s)
Downtrack	0.6096	0.00002862
Crosstrack	0.6096	0.00053427
Radial	0.1524	0.00013298

Dual-valued sensitivity coefficients arising from ε_r variations at t_0 (m_{ij} with $i = 1 \rightarrow 6$; $j = 1 \rightarrow 3$) appear in Table 23, and dual-valued sensitivity coefficients arising from ε_v variations at t_0 (m_{ij} with $i = 1 \rightarrow 6$; $j = 4 \rightarrow 6$) appear in Table 24. Note ε_r is directionally dependent and alters all three components of $\boldsymbol{r}$. Likewise, ε_v is directionally dependent and alters all three components of $\boldsymbol{v}$.

Table 23. Dual-valued sensitivity coefficients arising from ε_r variations at t_0 are presented with respect to nominal heliocentric J2KE elements at t_D.

t_0 Variations →	$\boldsymbol{r} \mp \varepsilon_r$ (downtrack)	$\boldsymbol{r} \mp \varepsilon_r$ (crosstrack)	$\boldsymbol{r} \mp \varepsilon_r$ (radial)
km^{-1} *EC* sensitivities	(-7.201E-06, -7.189E-06)	(-4.376E-07, -4.311E-07)	(-3.346E-05, -3.347E-05)
AU/km *QR* sensitivities	(2.218E-05, 2.216E-05)	(1.071E-06, 1.068E-06)	(3.898E-05, 3.900E-05)
day/km *TP* sensitivities	(7.174E-03, 7.178E-03)	(2.396E-04, 2.451E-04)	(-1.217E-02, -1.217E-02)
°/km *OM* sensitivities	(2.219E-04, 2.219E-04)	(-7.106E-03, -7.073E-03)	(-2.828E-04, -2.828E-04)
°/km *W* sensitivities	(1.001E-02, 1.001E-02)	(7.491E-03, 7.463E-03)	(-7.020E-03, -7.020E-03)
°/km *IN* sensitivities	(-1.976E-05, -1.976E-05)	(6.647E-04, 6.647E-04)	(2.421E-05, 2.421E-05)

Table 24. Dual-valued sensitivity coefficients arising from ε_v variations at t_0 are presented with respect to nominal heliocentric J2KE elements at t_D.

t_0 Variations →	$\boldsymbol{v} \mp \varepsilon_v$ (downtrack)	$\boldsymbol{v} \mp \varepsilon_v$ (crosstrack)	$\boldsymbol{v} \mp \varepsilon_v$ (radial)
s/km *EC* sensitivities	(7.847E-02, 7.847E-02)	(6.921E-04, 7.026E-04)	(6.623E-04, 6.637E-04)
AU/km/s *QR* sensitivities	(-1.133E-01, -1.133E-01)	(-1.703E-03, -1.717E-03)	(-2.839E-02, -2.839E-02)
day/km/s *TP* sensitivities	(1.299E+01, 1.299E+01)	(-3.855E-01, -3.834E-01)	(-1.938E+01, -1.938E+01)
°/km/s *OM* sensitivities	(2.068E-01, 2.068E-01)	(1.145E+01, 1.152E+01)	(-5.605E-01, -5.604E-01)
°/km/s *W* sensitivities	(-1.824E+00, -1.824E+00)	(-1.207E+01, -1.214E+01)	(-2.295E+01, -2.295E+01)
°/km/s *IN* sensitivities	(-1.785E-02, -1.785E-02)	(-1.042E+00, -1.042E+00)	(4.937E-02, 4.936E-02)

Apollo 11 S-IVB-506 Reconstruction

Using residual propellant dumps following TLI and CSM/LM ejection, the Apollo 11 S-IVB approached the Moon over its trailing hemisphere and obtained a gravity assist leading to disposal in interplanetary space. Table 25 data recount pertinent mission events through disposal.

Table 25. The following Apollo 11 mission events led to S-IVB disposal.

GET (hhh:mm:ss)	1969 GMT	Event
000:00:00	16 Jul 13:32:00	Launch [12, p. 286]
000:11:49	16 Jul 13:43:49	Earth orbit insertion following S-IVB Burn #1: H_A = +185.9 km, H_P = +183.2 km [12, p. 286]
002:50:13	16 Jul 16:22:13	TLI following S-IVB Burn #2 [12, p. 289]
003:15:23	16 Jul 16:47:23	CSM separation from S-IVB [12, p. 289] and epoch t_0 at final published S-IVB NAT elements [18, p. 4-10]
004:17:03	16 Jul 17:49:03	Mated CSM/LM is ejected from S-IVB [12, p. 289]
004:51:08	16 Jul 18:23:07	S-IVB post-TLI propulsive accelerations are initiated [12, p. 321]
005:17:00	16 Jul 18:49:00	Approximate midpoint of post-TLI S-IVB propulsive accelerations and epoch t_1
005:42:28	16 Jul 19:14:27	S-IVB post-TLI propulsive accelerations are terminated [12, p. 321]
078:42:00	19 Jul 20:14:00	S-IVB pericynthion passage and epoch t_2: H_P = +3379 km [18, p. 7-1]

Table 26. Nominal geocentric initial conditions for the Apollo 11 S-IVB EDTR are expressed as reported NAT elements [18, p. 4-10] and as equivalent J2K Cartesian components.

Epoch t_0 = 16 Jul 1969 at 197/16:47:23.0 GMT	
NAT Elements	**J2K Components**
h = +3815.2 nm	r_1 = -1214.275304 km
ϕ = +31.246°	r_2 = +13,257.838388 km
λ = -90.622°	r_3 = +1827.577578 km
s = 24,962.6 ft/s	v_1 = -5.831089559 km/s
γ = +45.148°	v_2 = +4.851662048 km/s
ψ = 93.758°	v_3 = +0.592090519 km/s

Table 26 nominal $\boldsymbol{r}$ and $\boldsymbol{v}$ are coasted from t_0 to t_1, where geocentric position and t_1 serve as initial boundary conditions in a perturbed Lambert problem whose final boundary conditions are t_2, selenocentric H_P = +3379 km [18, p. 7-1], and selenocentric λ = +68° inferred from t_2 mapped onto a lunar flyby trajectory plot [18, p. 7-5]. The plot's annotated "TOWARD EARTH" direction is assumed to also point at selenocentric λ = 0 while performing this mapping. Because the plot is two-dimensional and lies near the lunar equatorial plane, selenocentric ϕ at t_2 cannot be inferred from it. Furthermore, the plot indicates the t_2 pericynthion epoch is also that of S-IVB closest approach to the mated CSM/LM in low lunar orbit. Due to this unlikely coincidence, the λ = +68° final boundary condition is suspect and only serves as a preliminary value for further iterations in λ.

A solution to the t_1/t_2 Lambert problem is therefore sought such that deviation from final position is less than 0.001 km as selenocentric ϕ and λ at t_2 are iterated to achieve selenocentric γ near zero at t_2. In addition, a velocity increment $|\boldsymbol{\Delta v}|$ at t_1 is sought close to but slightly in excess of 36.3 m/s, the reported S-IVB longitudinal component of residual propellant dump velocity change [18, p. 7-2]. The $|\boldsymbol{\Delta v}|$ increment is computed as the vector difference between a perturbed Lambert solution's initial velocity minus velocity in the nominal EDTR as coasted from Table 26 initial conditions to t_1. Iteration results appear in Table 27.

Table 27. Results from evaluating multiple perturbed Lambert solutions over the t_1/t_2 arc are recorded as selenocentric ϕ and λ at t_2 are iterated. Selenocentric h = +3379 km at t_2 is held constant at its reported H_P value during this process. The ϕ = +10°; λ = +61° solution is adopted by the EDTR because its selenocentric γ is nearest to zero, a necessary and sufficient condition for pericynthion in a lunar flyby. Its $|\boldsymbol{\Delta v}|$ also slightly exceeds 0.0363 km/s, the reported primary component of velocity change imparted by residual propellant dumps in the t_1 time frame.

ϕ (deg)	λ (deg)	$\lvert\boldsymbol{\Delta v}\rvert$ (km/s)	γ (deg)
+20	+68	0.039246	+3.940
+10	+68	0.036901	+4.510
0	+68	0.037010	+4.288
-10	+68	0.039495	+3.289
-20	+68	0.043505	+1.570
+10	+63	0.036628	+1.231
+5	+63	0.037123	+1.183
+5	+62	0.036282	+0.512
+10	+61	0.036497	-0.097
+11	+61	0.036624	-1.103

From the ϕ = +10°; λ = +61° pericynthion "best fit" Lambert solution, J2K Cartesian components of the impulse at t_1 are computed as $\boldsymbol{\Delta v}$ = $[+0.03541676, +0.00384168, +0.00793096]^T$ km/s. This impulse is incorporated as an event in the Apollo 11 S-IVB nominal EDTR.

Reported S-IVB heliocentric orbit aphelion distance r_A = 151,860,000 km and perihelion distance r_P = 134,300,000 km [18, p. 7-8]. Figure 17 compares these reported apses with osculating values at hourly intervals during the nominal EDTR. As the S-IVB enters interplanetary space, Figure 17 indicates the degree to which reported apsis values are being approached asymptotically, a necessary condition for consistency.

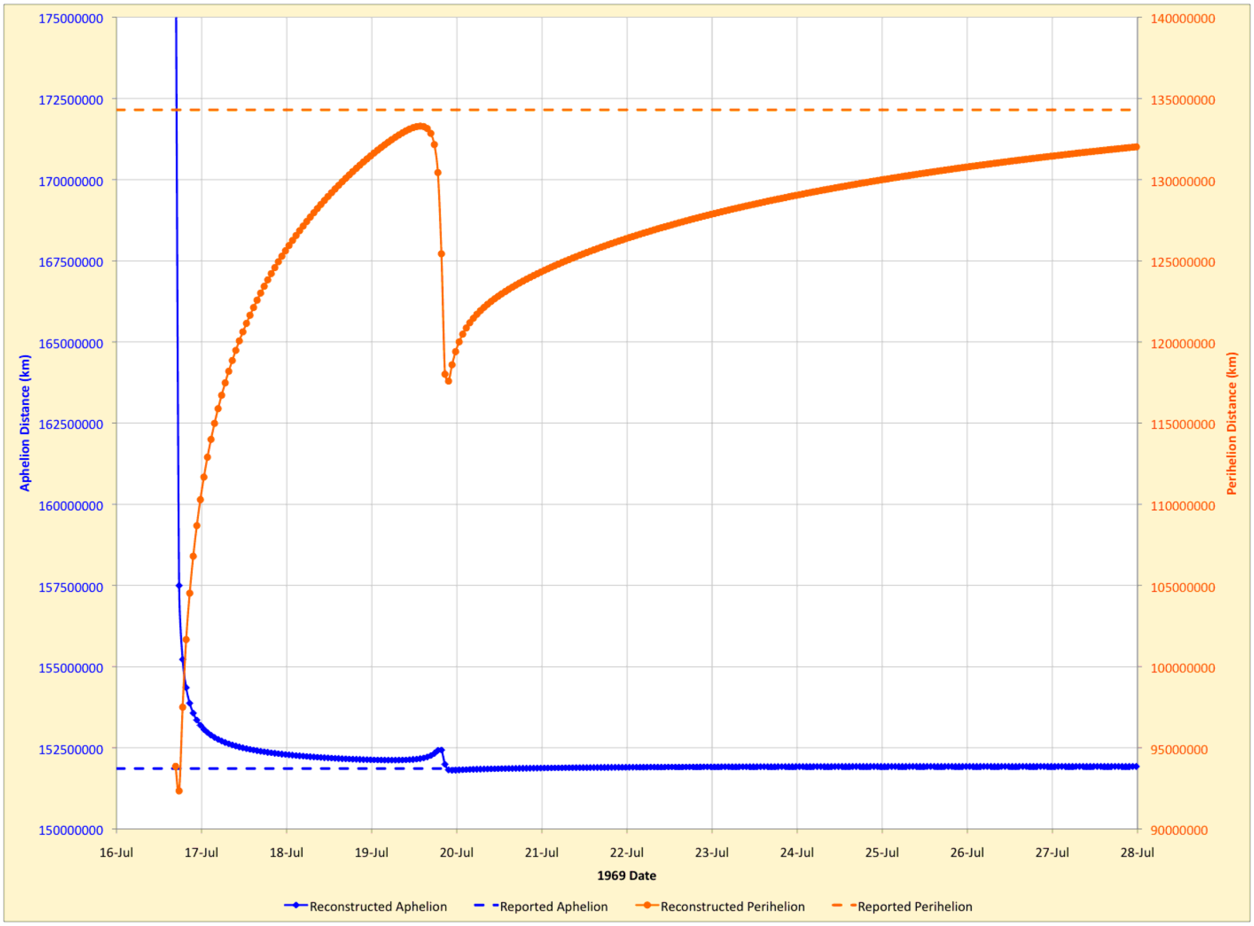

Figure 17. Apollo 11 S-IVB osculating aphelion (blue diamonds) and perihelion (orange dots) distances are plotted during nominal EDTR from 16 to 28 July 1969 GMT. Reported values for these apses [18, p. 7-8] are plotted as dashed lines of the corresponding color. As expected, each nominal apsis asymptotically approaches its reported value while the EDTR progresses toward interplanetary space. Rapidly varying EDTR apses on 19 July reflect the effects of lunar encounter.

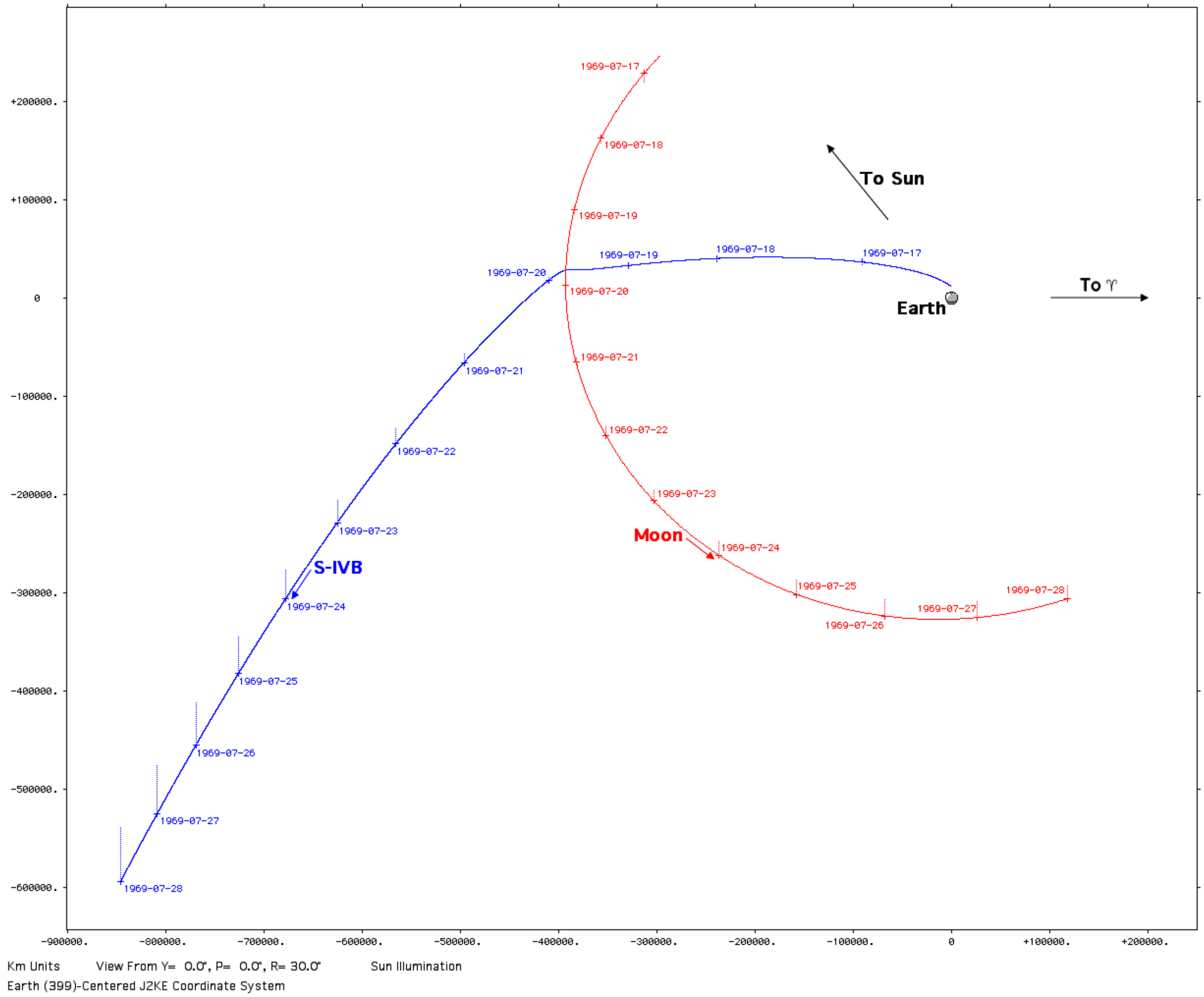

Figure 18. This geocentric inertial trajectory plot is viewed from ecliptic longitude 270°; latitude +60° and illustrates Apollo 11 S-IVB nominal EDTR. The departure asymptote lies nearly opposite Earth's heliocentric motion as inferred from the Sun's direction. Time ticks are at even GMT dates and annotated in year-month-day format. Dotted lines are projections onto the ecliptic plane.

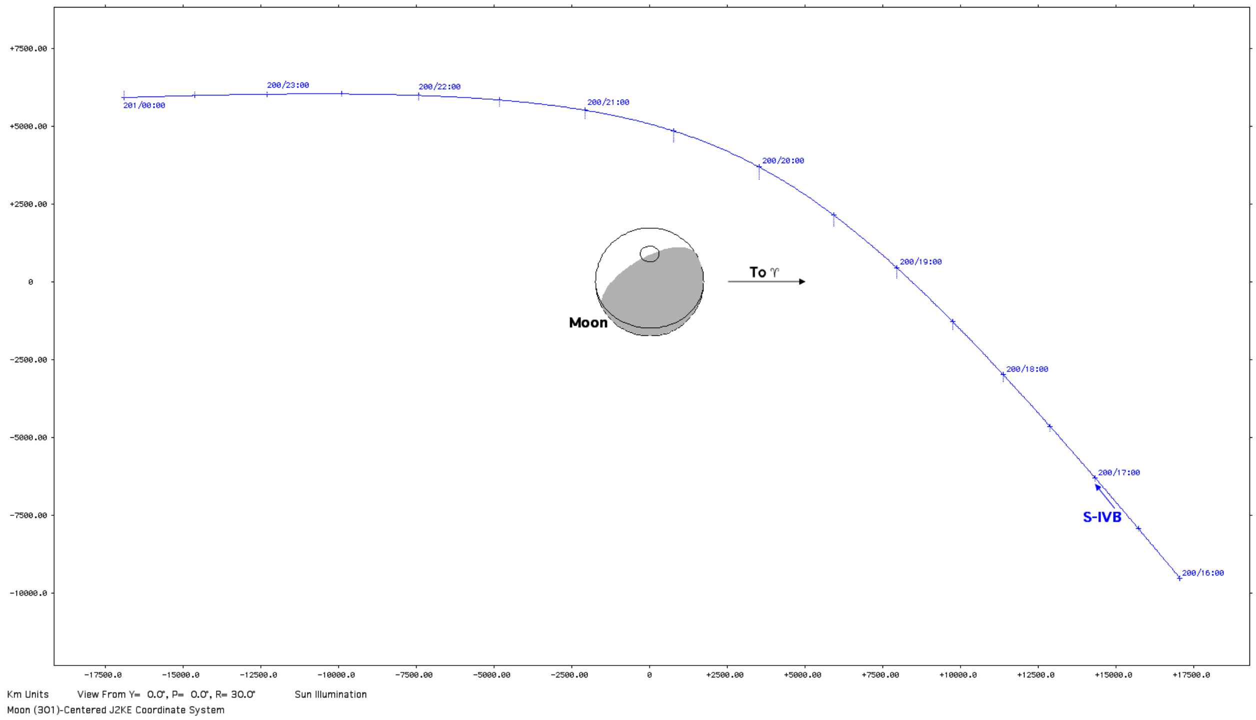

Figure 19. This inertial trajectory plot illustrates nominal Apollo 11 S-IVB EDTR selenocentric motion during 19 July 1969 GMT and is viewed from the same perspective as Figure 18 (ecliptic longitude 270°; latitude +60°). The Moon's shaded hemisphere is its nightside. Time tick annotations are at one-hour intervals in day-of-year/hh:mm format. Dotted lines are projections onto the ecliptic plane.

Table 28. Terminal geocentric position *r'* and velocity *v'* for the nominal Apollo 11 S-IVB EDTR are given with J2K Cartesian components.

Epoch t_D = 28.0 Jul 1969 GMT
r_1' = -846,172.698104 km
r_2' = -526,076.154082 km
r_3' = -349,270.077601 km
v_1' = -0.415383990 km/s
v_2' = -0.703944048 km/s
v_3' = -0.453189696 km/s

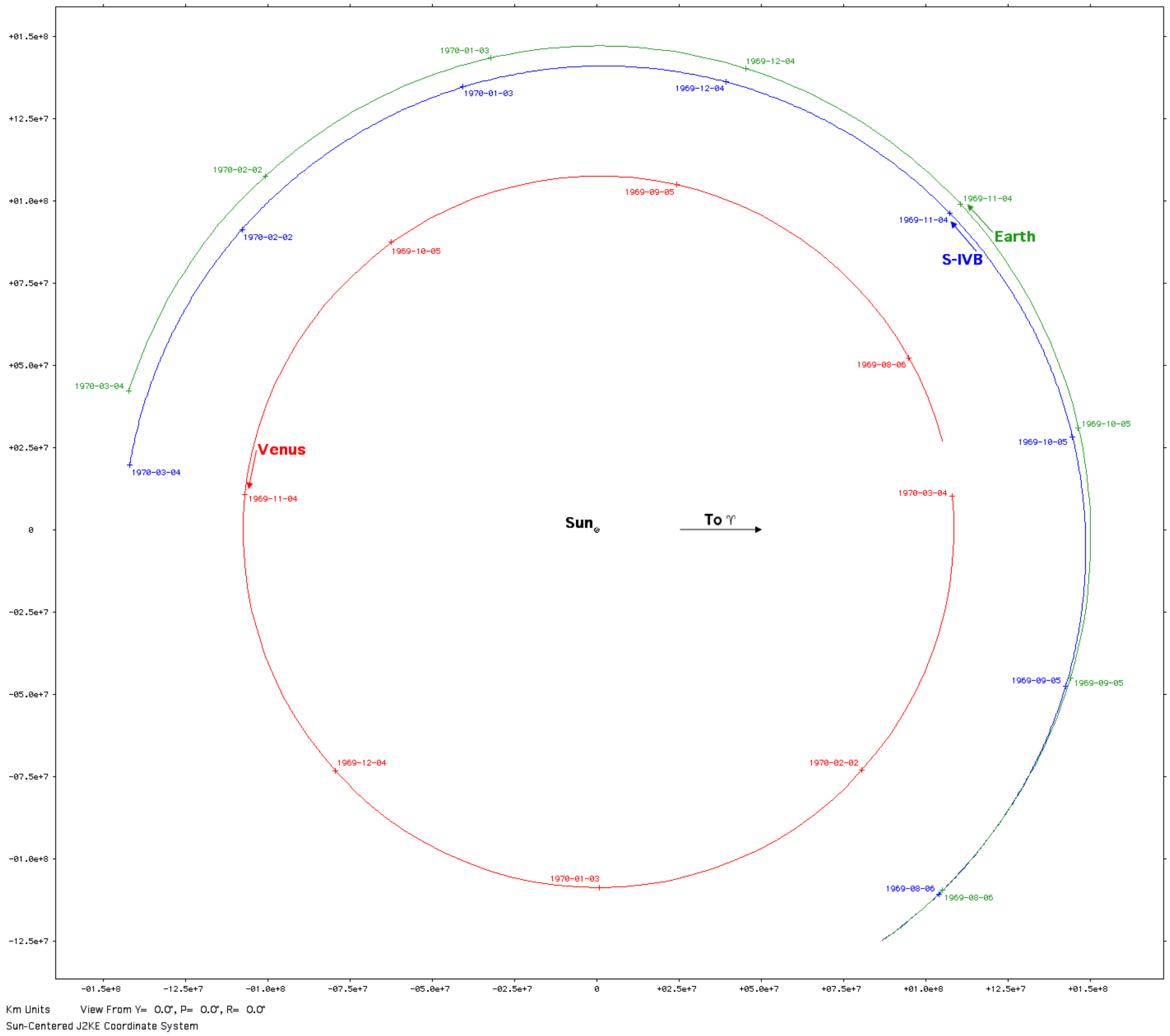

Figure 20. *Horizons* prediction of Apollo 11 S-IVB inertial heliocentric motion from Table 28 data is plotted with corresponding Earth and Venus motion for the first seven months following S-IVB disposal. Time ticks are at 30-day intervals and annotated in year-month-day format.

Total uncertainty associated with Table 26 Apollo 11 S-IVB $\boldsymbol{r}$ and $\boldsymbol{v}$ at t_0 is estimated to be $\varepsilon_r = \pm 1.5$ km in each position component and $\varepsilon_v = \pm 0.002$ km/s in each velocity component [18, p. 5-3]. Dual-valued sensitivity coefficients arising from ε_r variations at t_0 (m_{ij} with $i = 1 \rightarrow 6; j = 1 \rightarrow 3$) appear in Table 29, and dual-valued sensitivity coefficients arising from ε_v variations at t_0 (m_{ij} with $i = 1 \rightarrow 6; j = 4 \rightarrow 6$) appear in Table 30.

Table 29. Dual-valued sensitivity coefficients arising from ε_r variations at t_0 are presented with respect to nominal heliocentric J2KE elements at t_D.

t_0 Variations →	$r_1 \mp \varepsilon_r$	$r_2 \mp \varepsilon_r$	$r_3 \mp \varepsilon_r$
km^{-1} ***EC*** **sensitivities**	(3.464E-08, 3.496E-08)	(-8.708E-08, -8.672E-08)	(-5.091E-08, -5.059E-08)
AU/km *QR* sensitivities	(-1.032E-07, -1.038E-07)	(2.686E-07, 2.680E-07)	(1.593E-07, 1.588E-07)
day/km *TP* sensitivities	(-2.124E-04, -2.121E-04)	(5.811E-04, 5.813E-04)	(3.515E-04, 3.517E-04)
°/km *OM* sensitivities	(-8.650E-07, -7.756E-07)	(2.959E-06, 3.072E-06)	(7.175E-07, 8.155E-07)
°/km *W* sensitivities	(-2.149E-04, -2.149E-04)	(5.858E-04, 5.858E-04)	(3.550E-04, 3.551E-04)
°/km *IN* sensitivities	(-1.065E-06, -1.035E-06)	(3.104E-06, 3.141E-06)	(1.381E-06, 1.414E-06)

Table 30. Dual-valued sensitivity coefficients arising from ε_v variations at t_0 are presented with respect to nominal heliocentric J2KE elements at t_D.

t_0 Variations →	$v_1 \mp \varepsilon_v$	$v_2 \mp \varepsilon_v$	$v_3 \mp \varepsilon_v$
s/km *EC* sensitivities	(6.361E-04, 6.362E-04)	(1.537E-05, 1.538E-05)	(-2.270E-04, -2.266E-04)
AU/km/s *QR* sensitivities	(-1.124E-03, -1.124E-03)	(3.258E-04, 3.259E-04)	(5.988E-04, 5.983E-04)
day/km/s *TP* sensitivities	(1.246E-01, 1.248E-01)	(1.842E+00, 1.842E+00)	(9.875E-01, 9.876E-01)
°/km/s *OM* sensitivities	(1.697E-02, 1.704E-02)	(-5.890E-02, -5.883E-02)	(1.253E-01, 1.252E-01)
°/km/s *W* sensitivities	(-4.250E-02, -4.242E-02)	(1.858E+00, 1.858E+00)	(8.938E-01, 8.939E-01)
°/km/s *IN* sensitivities	(4.799E-04, 5.020E-04)	(-2.389E-02, -2.386E-02)	(5.967E-02, 5.968E-02)

Apollo 12 S-IVB-507 Reconstruction

Using residual propellant dumps following TLI and CSM/LM ejection, the Apollo 12 S-IVB was targeted to approach the Moon over its trailing hemisphere and obtain a gravity assist leading to disposal in interplanetary space. Although the dumps were performed according to plan, they were based on a post-TLI trajectory model failing to account for a shortfall in targeted TLI Δv [19, p. 7-1].

Consequently, these dumps over-corrected the actual post-TLI trajectory and resulted in a reported S-IVB pericynthion height more than 3.4 times greater than that being targeted [19, p. 7-5]. Reported pericynthion height exceeds the maximum threshold required of a lunar gravity assist to guarantee Earth departure for interplanetary space. As computed from an estimated S-IVB state vector 21 days after launch, reported osculating apogee and perigee distances are 895,600 and 121,090 km [19, p. 7-6], respectively.

Estimated S-IVB apogee distance is equivalent to 96% of Earth's gravitational sphere of influence radius in interplanetary space. The reported S-IVB disposal trajectory is therefore in a chaotic region of geocentric space and only loosely bound to Earth. This geocentric orbit instability is further compounded by reported perigee inside the Moon's orbit, indicating additional lunar encounters are possible after that targeted during Apollo 12 mission operations. Over prolonged time intervals of years, this S-IVB could easily drift into interplanetary space. Table 31 data recount pertinent mission events through disposal.

Table 31. The following Apollo 12 mission events led to S-IVB disposal.

GET (hhh:mm:ss)	1969 GMT	Event
000:00:00	14 Nov 16:22:00	Launch [12, p. 329]
000:11:44	14 Nov 16:33:44	Earth orbit insertion following S-IVB Burn #1: H_A = +185.4 km, H_P = +181.1 km [12, p. 331]
002:53:14	14 Nov 19:15:14	TLI following S-IVB Burn #2 [12, p. 333]
003:18:05	14 Nov 19:40:05	CSM separation from S-IVB [12, p. 333] and epoch t_0 at final published S-IVB NAT elements [19, p. 4-10]
004:13:01	14 Nov 20:35:01	Mated CSM/LM is ejected from S-IVB [12, p. 333]
004:26:40	14 Nov 20:48:40	S-IVB post-TLI propulsive accelerations are initiated [12, p. 333]
005:00:00	14 Nov 21:22:00	Approximate midpoint of post-TLI S-IVB propulsive accelerations and epoch t_1
005:33:43	14 Nov 21:55:43	S-IVB post-TLI propulsive accelerations are terminated [12, p. 355]
085:48:00	18 Nov 06:10:00	S-IVB pericynthion passage and epoch t_2: H_P = +5707 km [19, p. 7-1]

Table 32. Nominal geocentric initial conditions for the Apollo 12 S-IVB EDTR are expressed as reported NAT elements [19, p. 4-10] and as equivalent J2K Cartesian components.

Epoch t_0 = 14 Nov 1969 at 318/19:40:04.9 GMT	
NAT Elements	**J2K Components**
h = +3819.3 nm	r_1 = -102.095998 km
ϕ = +28.815°	r_2 = -11789.798010 km
λ = -79.537°	r_3 = +6465.310594 km
s = 24,865.5 ft/s	v_1 = +5.224395399 km/s
γ = +45.092°	v_2 = -5.198870663 km/s
ψ = 100.194°	v_3 = +1.765996671 km/s

Table 32 nominal $\boldsymbol{r}$ and $\boldsymbol{v}$ are coasted from t_0 to t_1, where geocentric position and t_1 serve as initial boundary conditions in a perturbed Lambert problem whose final boundary conditions are t_2 and selenocentric H_P = +5707 km [19, p. 7-1]. Unlike previous mission reports, Reference [19] contains no lunar flyby trajectory plot from which a final selenocentric λ boundary condition can be inferred at t_2.

A solution to the t_1/t_2 Lambert problem is therefore sought such that deviation from final position is less than 0.001 km as selenocentric ϕ and λ at t_2 are iterated to achieve selenocentric γ near zero at t_2. In addition, a velocity increment $|\boldsymbol{\Delta v}|$ at t_1 is sought close to but slightly in excess of 38.2 m/s, the reported S-IVB longitudinal component of residual propellant dump velocity change [19, p. 7-4]. The $|\boldsymbol{\Delta v}|$ increment is computed as the vector difference between a perturbed Lambert solution's initial velocity minus velocity in the nominal EDTR as coasted from Table 32 initial conditions to t_1. Iteration results appear in Table 33.

Table 33. Results from evaluating multiple perturbed Lambert solutions over the t_1/t_2 arc are recorded as selenocentric ϕ and λ at t_2 are iterated. Selenocentric h = +5707 km at t_2 is held constant at its reported H_P value during this process. The ϕ = -18.1°; λ = +45.3° solution is adopted by the EDTR because its selenocentric γ is nearest to zero, a necessary and sufficient condition for pericynthion in a lunar flyby. Its $|\Delta v|$ also slightly exceeds 0.0382 km/s, the reported primary component of velocity change imparted by residual propellant dumps in the t_1 time frame.

ϕ (deg)	λ (deg)	$\lvert\Delta v\rvert$ (km/s)	γ (deg)
0.0	60.0	65.610	+6.828
0.0	50.0	61.692	+0.217
-10.0	50.0	49.709	+2.054
-18.1	45.3	38.472	-0.006
-18.8	45.3	37.659	+0.075
-18.0	45.2	38.560	-0.084
-18.8	45.2	37.631	+0.008
-20.0	45.0	36.197	+0.009
-21.0	45.0	35.065	+0.115

From the ϕ = -18.1°; λ = +45.3° pericynthion "best fit" Lambert solution[††], J2K Cartesian components of the impulse at t_1 are computed as $\boldsymbol{\Delta v}$ = [-0.03134341, -0.01478300, +0.01670888]^T km/s. This impulse is incorporated as an event in the Apollo 12 S-IVB nominal EDTR.

[††] A flight note inserted prior to p. 13 in the Apollo 12 Flight Dynamics Officer (FDO) Log independently corroborates this solution. In 1999, the author consulted the original copy of this log archived at NASA-JSC while researching Apollo 12 trajectory operations. Selenocentric S-IVB pericynthion conditions are given as h = 3091.01 nm (5724.55 km), ϕ = -17.40°, and λ = +45.38° in the flight note. Because these values were obtained during mission operations, they are deemed less accurate than those derived in this paper based on post-flight reports.

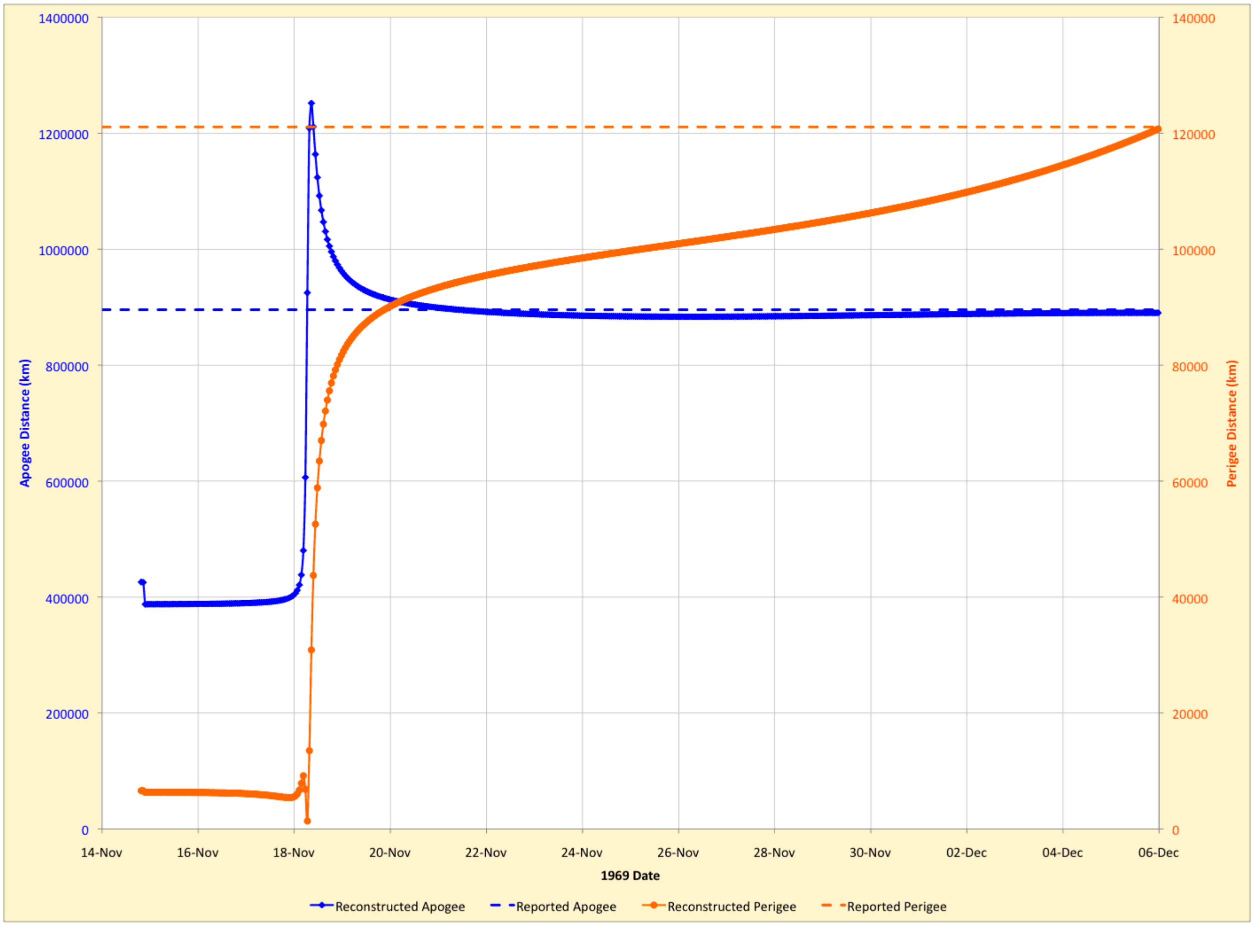

Figure 21. Apollo 12 S-IVB osculating apogee (blue diamonds) and perigee (orange dots) distances are plotted during nominal EDTR from 14 November to 6 December 1969 GMT. Reported values for these apses [19, p. 7-6], based on a 5 December projected state vector, are plotted as dashed lines of the corresponding color. Nominal perigee does not asymptotically approach its reported value as the EDTR progresses toward t_D because this epoch is near apogee, where strong solar perturbations are raising perigee. Rapidly varying EDTR apses on 18 November reflect the effects of lunar encounter.

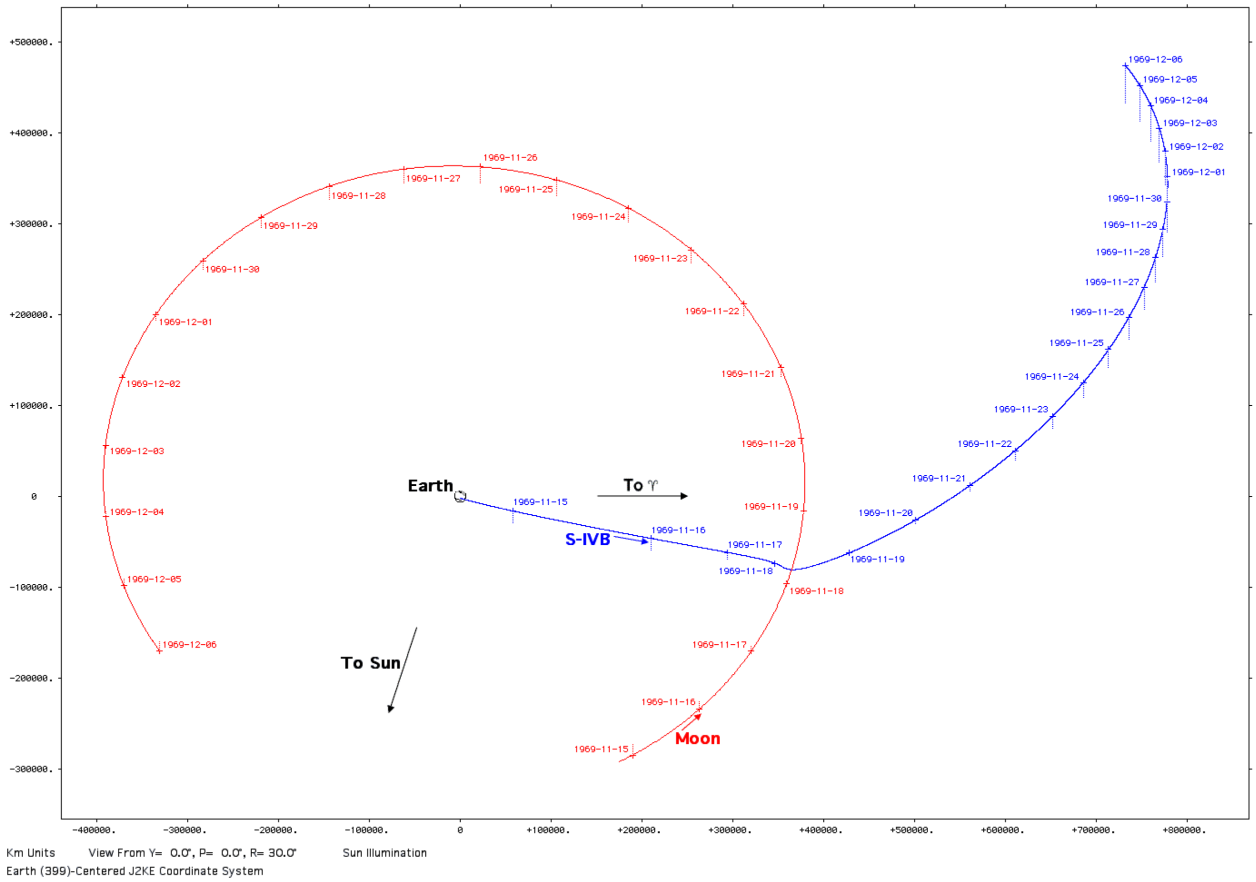

Figure 22. This geocentric inertial trajectory plot is viewed from ecliptic longitude 270°; latitude +60° and illustrates Apollo 12 S-IVB nominal EDTR. Time ticks are at even GMT dates and annotated in year-month-day format. Dotted lines are projections onto the ecliptic plane.

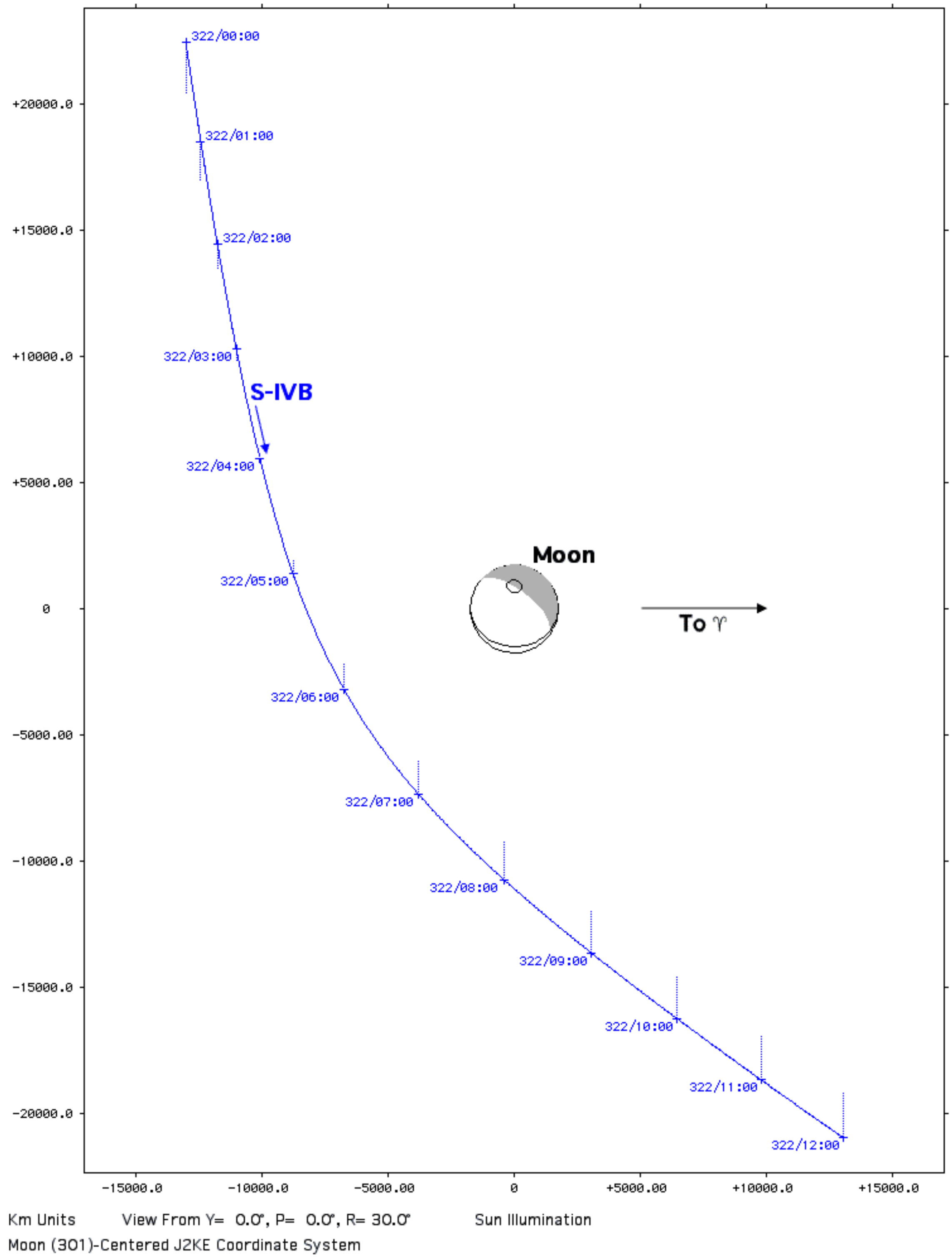

Figure 23. This inertial trajectory plot illustrates nominal Apollo 12 S-IVB EDTR selenocentric motion during 18 November 1969 GMT and is viewed from the same perspective as Figure 22 (ecliptic longitude 270°; latitude +60°). The Moon's shaded hemisphere is its nightside. Time tick annotations are at one-hour intervals in day-of-year/hh:mm format. Dotted lines are projections onto the ecliptic plane.

Table 34. Terminal geocentric position *r*' and velocity *v*' for the nominal Apollo 12 S-IVB EDTR are given with J2K Cartesian components.

Epoch t_D = 6.0 Dec 1969 GMT
r_1' = +732,393.597665 km
r_2' = +424,512.352359 km
r_3' = +274,950.877995 km
v_1' = -0.194841341 km/s
v_2' = +0.231531578 km/s
v_3' = +0.124914799 km/s

Total uncertainty associated with Table 32 Apollo 12 S-IVB ***r*** and ***v*** at t_0 is estimated to be ε_r = ±0.75 km in each position component and ε_v = ±0.0015 km/s in each velocity component [19, p. 5-3]. Dual-valued sensitivity coefficients arising from ε_r variations at t_0 (m_{ij} with $i = 1 \rightarrow 6$; $j = 1 \rightarrow 3$) appear in Table 35, and dual-valued sensitivity coefficients arising from ε_v variations at t_0 (m_{ij} with $i = 1 \rightarrow 6$; $j = 4 \rightarrow 6$) appear in Table 36.

Table 35. Dual-valued sensitivity coefficients arising from ε_r variations at t_0 are presented with respect to nominal heliocentric J2KE elements at t_D.

t_0 **Variations** →	$r_1 \mp \varepsilon_r$	$r_2 \mp \varepsilon_r$	$r_3 \mp \varepsilon_r$
km^{-1} *EC* sensitivities	(-6.224E-08, -6.345E-08)	(6.880E-07, 6.868E-07)	(-2.950E-07, -2.962E-07)
AU/km *QR* sensitivities	(1.772E-08, 1.788E-08)	(-1.568E-07, -1.566E-07)	(5.948E-08, 5.962E-08)
day/km *TP* sensitivities	(-5.401E-05, -5.449E-05)	(4.854E-04, 4.849E-04)	(-1.810E-04, -1.815E-04)
°/km *OM* sensitivities	(2.464E-04, 2.486E-04)	(-1.900E-03, -1.898E-03)	(8.979E-04, 9.000E-04)
°/km *W* sensitivities	(-3.020E-04, -3.047E-04)	(2.401E-03, 2.399E-03)	(-1.085E-03, -1.088E-03)
°/km *IN* sensitivities	(-7.618E-07, -7.636E-07)	(3.018E-06, 3.017E-06)	(-2.214E-06, -2.216E-06)

Table 36. Dual-valued sensitivity coefficients arising from ε_v variations at t_0 are presented with respect to nominal heliocentric J2KE elements at t_D.

t_0 **Variations** →	$v_1 \mp \varepsilon_v$	$v_2 \mp \varepsilon_v$	$v_3 \mp \varepsilon_v$
s/km *EC* sensitivities	(1.728E-03, 1.727E-03)	(2.777E-03, 2.777E-03)	(3.305E-04, 3.290E-04)
AU/km/s *QR* sensitivities	(-3.028E-04, -3.027E-04)	(-7.104E-04, -7.104E-04)	(-2.859E-04, -2.857E-04)
day/km/s *TP* sensitivities	(9.562E-01, 9.558E-01)	(2.239E+00, 2.239E+00)	(9.659E-01, 9.652E-01)
°/km/s *OM* sensitivities	(-3.019E+00, -3.019E+00)	(-6.370E+00, -6.374E+00)	(1.212E+00, 1.217E+00)
°/km/s *W* sensitivities	(4.010E+00, 4.009E+00)	(8.678E+00, 8.680E+00)	(-2.267E-01, -2.329E-01)
°/km/s *IN* sensitivities	(-3.701E-03, -3.702E-03)	(-8.052E-04, -8.080E-04)	(-2.251E-02, -2.250E-02)

If the nominal EDTR is extended beyond t_D, lunar impact occurs on 24 December 1969 at 03:14:41 GMT. When extended beyond t_D, 11 of the 12 sensitivity coefficient trajectories also impact the Moon on this date, but the one with $v_2 + \varepsilon_v$ initial conditions at t_0 has selenocentric H_P = +106 km. More rigorous Monte Carlo analysis, together with solar radiation pressure modeling, will undoubtedly show S-IVB impact on 24 December 1969 is not a certainty.

The S-IVB's fate on 24 December 1969 is independently verified by consulting event catalog data from the Apollo 12 Passive Seismic Experiment (PSE) [20] recorded on this date. Although the Apollo 12 seismometer was operational throughout 24 December 1969 GMT, no impact event is recorded. Those seeking to determine whether or not the S-IVB evaded impact during other lunar encounters after 24 December 1969 are encouraged to consult PSE data at those times. These data may be obtained via "guest" login at ftp.ig.utexas.edu/pub/PSE/catsrepts (accessed 27 June 2012). Reference the ReadMe.txt file at this location for introductory information.

Conclusion

Six Apollo Program components targeted for disposal in interplanetary space during 1968 and 1969 have undergone trajectory reconstruction as documented in this paper. The first five of these components appear to have achieved heliocentric orbits consistent with the Aten NEO group[‡‡]. An Aten crosses Earth's orbit but has a period less than Earth's. This outcome is not surprising because four of these components departed Earth's vicinity constrained by proximity to the Moon while near its first quarter phase. At this point in the lunar month, the Moon trails Earth in their respective heliocentric orbits. Earth departure in the first quarter direction therefore imparts an initially retrograde heliocentric motion and a shorter period to the disposal trajectory with respect to Earth.

The fifth reconstructed Aten orbit arises from happenstance because Apollo 9 never targeted the Moon. However, this mission's S-IVB was injected on an Earth escape trajectory from a location near local sunrise, resulting in a geocentric departure direction opposed to Earth's heliocentric motion (reference Figure 7).

Because the Apollo 12 S-IVB did not immediately depart Earth's vicinity due to a disposal targeting error, its fate is indeterminate with respect to this paper's scope. The trajectory reconstruction documented by this paper ends in a chaotic geocentric state with potential for collision with the Earth or Moon, along with the possibility of ejection into heliocentric orbit after a lunar encounter. This chaotic state is consistent with those observed in connection with object J002E3 circa late 2002, as documented in the report at http://neo.jpl.nasa.gov/news/news135.html (accessed 23 June 2012).

Acknowledgments

The study documented by this paper would not have been possible without interest in its findings from Don Yeomans of JPL's Solar System Dynamics group (SSD) and Lindley Johnson, NEO Observations Program Executive at NASA Headquarters. Technical correspondence with Jon Giorgini at SSD is gratefully acknowledged and substantially contributed to this paper's integrity.

[‡‡] Aten orbits should be regarded as only the initial heliocentric state of the first five Apollo Program objects disposed in interplanetary space. Over decades of time since disposal, orbit perturbations (particularly during close Earth encounters) can dramatically change any of the initial heliocentric orbits documented in this paper.

References

[1] NRC Committee to Review Near-Earth Object Surveys and Hazard Mitigation Strategies, *Defending Planet Earth: Near-Earth Object Surveys and Hazard Mitigation Strategies*, The National Academies Press, Washington, D.C., 2010.[§§]

[2] Barbee, B.W., Mink, R.G., Adamo, D.R., and Alberding, C.M., "Methodology and Results of the Near-Earth Object (NEO) Human Space Flight (HSF) Accessible Targets Study (NHATS), AAS 11-444, *Volume 142 of the Advances in the Astronautical Sciences*, Univelt, San Diego, pp. 613-632, 2011.

[3] Adamo, D.R. and Barbee, B.W., "Why Atens Enjoy Enhanced Accessibility for Human Space Flight", AAS 11-449, *Volume 142 of the Advances in the Astronautical Sciences*, Univelt, San Diego, pp. 709-728, 2011.

[4] Adamo, D.R., "Apollo 13 Trajectory Reconstruction via State Transition Matrices", *Journal of Guidance, Control, and Dynamics*, Vol. 31, No. 6, AIAA, Washington, D.C., pp. 1772-1781, 2008.

[5] McCurdy, R.D., *Apollo/Saturn V Postflight Trajectory - AS-503*, D5-15794, The Boeing Company, 1969.

[6] Parker, S.P., *McGraw-Hill Dictionary of Scientific and Technical Terms*, Sixth Edition, McGraw-Hill, Columbus, OH, 2002.

[7] Mission Evaluation Team, *Apollo 8 Mission Report*, MSC-PA-R-69-1, NASA Manned Spacecraft Center, Houston, TX, 1969.

[8] TRW Systems Group, *Apollo 8 Mission Report Supplement 1: Trajectory Reconstruction and Postflight Analysis*, MSC-PA-R-69-1 Supplement 1, NASA Manned Spacecraft Center, Houston, TX, 1969.

[9] Adamo, D.R., "A Precision Orbit Predictor Optimized for Complex Trajectory Operations", AAS 03-665, *Volume 116 of the Advances in the Astronautical Sciences*, Univelt, San Diego, pp. 2567-2586, 2003.

[10] Giorgini, J.D., Yeomans, D.K., Chamberlin, A.B., Chodas, P.W., Jacobson, R.A., Keesey, M.S., Lieske, J.H., Ostro, S.J., Standish, E.M., Wimberly, R.N., "JPL's On-Line Solar System Data Service", *Bulletin of the American Astronomical Society*, Vol. 28, No. 3, p. 1158, 1996.[***]

[11] Anawalt, R.A. and Boskenberg, A., *The Astronomical Almanac for the Year 1989*, U.S. Government Printing Office, Washington, D.C., 1988.

[12] Orloff, R.W. and Harland, D.M., *Apollo: The Definitive Sourcebook*, Springer-Praxis, Chichester, UK, 2006.

[13] Seidelmann, P. K., Abalakin, V. K., Bursa, M., Davies, M. E., de Bergh, C., Lieske, J. H., Oberst, J., Simon, J. L., Standish, E. M., Stooke, P., and Thomas, P. C., “Report of the IAU/IAG Working Group on Cartographic Coordinates and Rotational Elements of the Planets and Satellites: 2000”, *Celestial Mechanics and Dynamical Astronomy*, Vol. 82, No. 1, pp. 83–111, 2002.

[14] McCurdy, R.D., *Apollo/Saturn V Postflight Trajectory - AS-504*, D5-15560-4, The Boeing Company, 1969.

[§§] A PDF file of this document may be downloaded from http://www.nap.edu/catalog/12842.html (accessed 10 April 2012).

[***] For further information on using this service, see http://ssd.jpl.nasa.gov/?horizons (accessed 10 April 2012).

[15] McCurdy, R.D., *Apollo/Saturn V Postflight Trajectory - AS-505*, D5-15560-5, The Boeing Company, 1969.
[16] Mission Evaluation Team, *Apollo 10 Mission Report*, MSC-00126, NASA Manned Spacecraft Center, 1969.
[17] Adamo, D.R., "The Elusive Human Maximum Altitude Record", *Quest: the History of Spaceflight Quarterly*, Vol. 16, No. 4, pp. 37-41, 2009.
[18] Krausse, S.C., *Apollo/Saturn V Postflight Trajectory - AS-506*, D5-15560-6, The Boeing Company, 1969.
[19] Krausse, S.C., *Apollo/Saturn V Postflight Trajectory - AS-507*, D5-15560-7, The Boeing Company, 1970.
[20] Nakamura, Y., Latham, G.V., Dorman, H.J., and Harris, J.E., "Passive seismic experiment long-period event catalog, Final version, 1969 day 202 - 1977 day 273", 314 pp., Galveston Geophysics Laboratory, Galveston, University of Texas Institute for Geophysics Technical Report No. 18, 1981.[†††]

[†††] An updated version is available via guest login from ftp.ig.utexas.edu/pub/PSE/catsrepts.